Journal Name

ARTICLE

Iron (III) bromide catalyzed bromination of 2-*tert*-butylpyrene and corresponding positions-dependent aryl-functionalized pyrene derivatives

Xing Feng,[a,b] Jian-Yong Hu,[b,c] Hirotsugu Tomiyasu,[b] Zhu Tao,[d] Carl Redshaw,[e] Mark R.J. Elsegood,[f] Lynne Horsburgh,[f] Simon J. Teat,[g] Xian-Fu Wei,[a] and Takehiko Yamato[*b]

The present work probes the bromination mechanism of 2-*tert*-butylpyrene (**1**), which regioselectively affords mono-, di-, tri-, and tetra-bromopyrenes, by theoretical calculation and detailed experimental methods. Bromine atom may directed to the K-region (positions 5- and 9-) instead of the more reactive positions 6- and 8-position in the presence of iron powder. In this process, $FeBr_3$ plays a significant role to release of steric hindrance or lowing the activation energy of the rearrangement. The intermediate bromopyrene derivatives were isolated and confirmed by ^{1}H NMR spectra, mass spectroscopy and elemental analysis. Further evidence on substituent positions originated from a series of aryl substituted pyrene derivatives, which were obtained from the corresponding bromopyrenes on reaction with 4-methoxy- phenylboronic acid by a Suzuki-Miyaura cross-coupling reaction. All of Positions-dependent aryl-functionalized pyrene derivatives are characterized by single X-ray diffraction, ^{1}H/^{13}C NMR, FT-IR and MS, and offered a straightforward proof to support our conclusion. Furthermore, the photophysical properties of series of compounds were confirmed by fluorescence and absorption, as well as by fluorescence lifetime measurements.

Introduction

Pyrene and its derivatives[1] belong to a classical family of polycyclic aromatic hydrocarbons (PHAs) that have been extensively investigated for light-emitting device applications over recent years. This interest stems from their inherent chemical and photochemical characteristics, in particular an excellent deep blue chromophore which exhibits great chemical stability and high charge carrier mobility. However, owing to its planar structure, pyrene has a strong tendency to form π-aggregates/excimers, which, in-turn, leads to an excimer emission band and the quenching of fluorescence in condensed media and a resulting low fluorescence quantum yield. With this in mind, enormous effort has been paid towards exploring new methods to functionalize the pyrene-core for developing molecular materials and applications thereof.

In general, due to the presence of nodal planes located at the 2- and 7-positions in both the highest occupied molecular orbital's (HOMO) and the lowest unoccupied molecular orbital's (LUMO) of pyrene, substituting pyrene at the 2- and/or 2,7-positions is more difficult compared to other positions (such as 1-, 3-, 6- and 8-positions (active site)).[2] Thus, there are few examples which focus on substituting at the 2- and 7-positions of pyrene by borylation,[3] bromination,[4] nitration,[5] oxidation[6] and *tert*-butylation.[7] On the other

hand, the active sites, namely the 1-, 3-, 6-, and 8-positions have been thoroughly examined and the products used in a variety of applications as optical materials.[1a,1b] Since we first reported[8] the oxidation of pyrene at the K-region (4-, 5-, 9- and 10-positions) in 1997 by stepwise synthetic methods, the K-region also has been explored as a convenient synthetic route to the ketone[9] and used for preparing pyrene-fused azaacene derivatives for application inorganic semiconductors.[10]

As previously mentioned, bromopyrenes are significant intermediate compounds which play an important role in modern organic chemistry, not only for synthetic methodology, but also for advanced optoelectronic materials. Commonly, the 1-, 3-, 6-, and 8-positions of pyrene preferentially undergo electrophilic aromatic substitution (S_EAr) reactions. Therefore, mono-, bis-, tri-, and tetrakis-substituted pyrenes were synthesized for organic electronic devices[1] and fluorescence probes.[11] For example, Thummel et al.[12] discussed the crystal packing of 1,3-, 1,6-, 1,8-, and 2,7-bis(2-[1,10]phenanthrolinyl)pyrenes and their use as pyrene-bridging ligands in ruthenium(II) chemistry, as evidenced by ^{1}H NMR spectra and single-crystal X-ray crystallography. Sankararaman[13] and co-workers reported a pyrene octaaldehyde derivative from 1,3,6,8-tetrabromopyrene, which can cause molecular aggregations in nonpolar solvents and in the solid-state through cooperativity of the

intermolecular π-π stacking and C–H⋯O interactions, which has potential application in the field of molecular optoelectronics. Chow[14] and co-workers synthesized sterically congested tetraaryl-pyrenes as efficient blue emitters that exhibited pure-blue electroluminescence and formed respectable organic light-emitting diodes (OLEDs). More recently, Konishi[15] and co-workers systematically alkylated the active sites, namely the 1-, 3-, 6-, and 8-positions of pyrene, and investigated the effects of the number of alkyl substituents on the photophysical properties of the pyrene chromophores. Recently, we reported a new type of fluorescent sensor based on a pyrene-linked triazole-modified hexahomotrioxa-calix[3]arene, which used the 1-pyrenyl moiety for selectively detecting Zn^{2+} and $H_2PO_4^-$ ions in neutral solutions.[16]

Bromination of the pyrene not only occurred at the active sites of 1-, 3-, 6-, and 8-positions, but also substitution occurred at the K-region, namely the 4-, 5-, 9-, and 10-positions. For instance, our group reported a series of pyrene-based cruciform/hand-shaped light-emitting monomers with highly emissive pure-blue fluorescence from tetrabromo/pentabromopyrene.[17] Very recently, we explored a new bromide precursor, 1,3,5,9-tetrabromo-7-*tert*-butylpyrene,[18] prepared via bromination of 2-*tert*-butylpyrene (**1**) in CH_2Cl_2 at room temperature using iron powder as the catalyst.

About twenty years ago, we reported a FeBr$_3$-catalyzed rearrangement of a pyrene-based material in which the bromine atom was transferred from the active site (1-position) to the K-region (4-position), *ie* bromination of 2,7-di-*tert*-butylpyrene with 1.1 mole equiv. of bromine in the presence of iron powder to afford 1-bromo-2,7-di-*tert*-butylpyrene, which can be further brominated with excess bromine in the presence of FeBr$_3$-catalyzed, and afforded 4,5,9,10-tetrabromo-2,7-di-*tert*-butylpyrene (Scheme 1).[8] However, the detailed bromination mechanism still remains unclear.
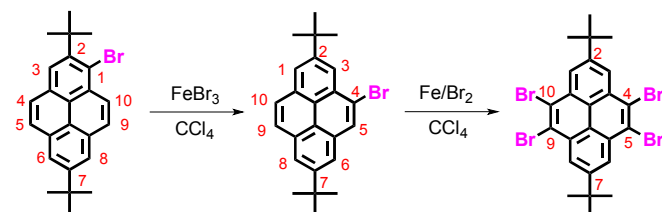
Scheme 1. FeBr$_3$-catalyzed rearrangement to afford 4,5,9,10-tetrabromo-2,7-di-*tert*-butylpyrene.

Interestingly, we recently succeeded in developing the bromide precursor 1,3,5,9-tetrabromo-7-*tert*-butylpyrene from 2-*tert*-butyl-pyrene (**1**) using iron-powder catalysis.[18] We speculated that the sequence of reactions involved a stepwise bromination process from the 1-, 3-, 5-, to the 9-position. In this case, it seemed easy to understand that the bromination reactions of the pyrene preferentially occurred at the active sites of the 1- and 3-positions owing to the *tert*-butyl group protecting the ring against electrophilic attack at the 6- and 8-positions.[22] Following this, as expected, the next step would be to substitute regioselectively at the 5- and 9-positions, which should be favoured given that the bromine atoms substituted at the 1- and 3-positions would sterically hinder the 4- and 10-positions. However, further experimental results revealed that the reaction process was more complicated than our initial predictions.

It is well known that bromination reactions can be violent and complex processes, thus to investigate the bromination mechanism is far from simple, because it is difficult to capture the transition state or a transition state analogue by experimental methods. Given this, the mechanism of electrophilic substitution was generally investigated by kinetic and stereochemical studies, or by theoretical analyses.[23] In additional, if the experimental conditions cannot be well controlled, then the final components will be complicated and hard to characterize.[24] In this paper, we present the first example of the systematic exploration of the bromination rearrangement reaction of pyrene affording the mono-, di-, tri-, and tetra-bromopyrenes by detailed experimental procedures and theoretical calculation. And the corresponding positions-dependent arylpyrenes derivatives containing the 4-methoxyphenyl group were synthesized from the corresponding bromopyrenes via a Suzuki-Miyaura cross-coupling reaction, which was characterized by single crystal X-ray diffraction and ^{1}H NMR spectroscopy. The detailed results have strongly supported the bromo-substituted positions in the pyrene ring as previous assumption. Furthermore, the effects of the methoxyphenyl group (both number and the substitution pattern) on their photophysical properties, as well as for their molecular packing, were investigated.

Results and discussion

Stoichiometric bromination of 2-*tert*-butylpyrene (1)

A three-neck round bottom flask fitted with a dropping funnel and a CaCl$_2$ drying tube, was filled with **1** (200 mg, 0.78 mmol) in 20 mL of CH_2Cl_2 and was stirred for 30 min. at 0 °C. A solution of Br$_2$ (depending on stoichiometric ratio) in 5 mL of CH_2Cl_2 was added drop-wise. After the addition of bromine was completed, the mixture was warmed to room temperature (28 °C) and stirred for 5 h. The crude product was washed with hot hexane and the yields of products are compiled in Table 1.
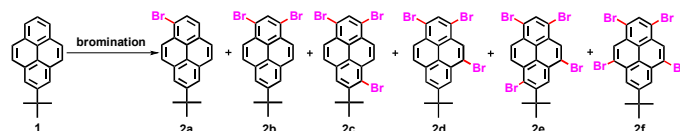
Scheme 2. Bromination of 2-*tert*-butylpyrene for **2**.

The synthesis of the key intermediate bromopyrenes is shown in Scheme 2. 1-Bromo-7-*tert*-butylpyrene (**2a**) and 1,3-dibromo-7-*tert*-butylpyrene (**2b**) have been synthesized with two kinds of bromination reagents and used to achieve the chemical modifications of the pyrenes for the required products.[22] Firstly, 1) a mixture of **1** and 1.0 equiv. bromine in CH_2Cl_2 at 28 °C in the presence of an iron powder catalyst, afforded **2a** in 83% yield; in the other hand, in the absence of iron powder, mixture of 1 and 1.0 equiv. bromine in CH_2Cl_2 at -78 °C afforded **2a** in 75% yield[22b]; 2) A mixture of **1** and BTMABr$_3$ (1.0 equiv.) in CH_2Cl_2 at 28 °C afforded the desired product **2a** in 84% yield. 3) According to reported,[22b] a mixture of Br$_2$ and **1** in anhydrous CH_2Cl_2 at -78 °C afforded **2a** in 89% yield in the absence of iron powder; however, in the presence of iron powder, a mixture of **1** and 2.0 equiv. of bromine at 28 °C afforded a mixture

**Table 1** Bromination of 2-*tert*-butylpyrene **1** under the various experimental conditions.[a]

Run	Substrate	Reagents	Reagents/**1** (mole rate)	Products (%)
1	**1**	Br_2-Fe	1.0	**2a** [83]
2	**1**	BTMABr$_3$	1.0	**2a** [84]
3	**1**	Br_2-Fe	2.0	**2a** [50], **2b** [35]
4	**1**	BTMABr$_3$	3.5	**2b** [76]
5	**1**	Br_2	3.9	**2c** [65]
6	**1**	Br_2-Fe	3.0	**2d** (25), **2f** (50)[b]
7	**1**	Br_2-Fe	6.0	**2f** [84]
8	**2c**	Br_2-Fe	2.5	**2e** (70), **2f** (30)[b]
9	**2e+2f**	Br_2-Fe	2.9	**2e** (25), **2f** (75)[b]

[a] The isolated yields are shown in square bracket. [b] Yields were determined by ^{1}H NMR analysis and shown in parentheses.

2a in 50% yield and **2b** in 35% yield. 4) A mixture of **1** and BTMABr$_3$ (3.5 equiv.) in CH_2Cl_2 at 28 °C afforded the desired product **2b** in 76% yield. Similarly, 5) for comparison, we synthesized 1,3,6-tribromo-7-*tert*-butylpyrene (**2c**) in the absence of iron powder in 65% yield according to the reported procedure.[25] 6) When **1** was mixed with stoichiometric Br$_2$ (1:3~5) under the same experimental conditions, the intermediate product 1,3,5-tribromo-7-*tert*-butylpyrene (**2d**) was obtained with **2f**, which could not be separated from the crude compound by column chromatography. We attempted to isolate both **2d** and **2f** in pure form by high-performance liquid chromatography (HPLC) but failed. 7) When the same reaction was carried out with 6.0 equiv. of bromine in the presence of iron powder, the Lewis acid-catalyzed rearrangement of bromine was observed to give 1,3,5,9-tetrabromo-7-*tert*-butylpyrene **2f** in 84% yield.[18] It seems that compound **2f** might be formed by the isomerization of compound **2c** under FeBr$_3$-catalyzed, which should be produced from bromine and iron powder present during the bromination. 8) Reaction of **2c** with Br$_2$ (1:2.5) was carried out in the presence of iron powder. A mixture of bromides 1,3,5,8-tetrabromo-7-*tert*-butylpyrene **2e** and 1,3,5,9-tetrabromo-7-*tert*-butylpyrene **2f** was obtained in the ratio of 7:3 (determined by their[1]H NMR spectra analysis); 9) when mixture of **2e** and **2f** was treated with 2.5 equiv. of bromine in the presence of iron powder in CH_2Cl_2 solution at 28 °C for 8 h, the expected product, **2f** was obtained in 75% yield. 10) However, attempted isomerization of compound **2e** to **2f** with other Lewis acids, such as TiCl$_4$, AlCl$_3$ or FeCl$_3$, performed under the same reaction conditions failed; only the starting compound **2e** was quantitatively recovered. Brominations of compound **1** in the presence of iron powder to afford the bromo-substituted pyrene derivatives **2** were carried out under various reaction conditions and the detailed results are summarized in Table 1.

Regioselective bromination mechanism of 2-*tert*-butylpyrene (1)

From previous experimental section, **2a**, **2b**, and **2c** were prepared that is not depending on the presence of iron (III) bromine, instead, the stoichiometric ratio of bromine reagent. This process is classical electrophilic substitution reaction. This result is strongly attributed to the high reactivity of the 1-, 3-, 6- and 8-positions in the pyrene ring. However, in the following bromination reactions for **2d**, **2e** and the role played by the FeBr$_3$-induced rearrangement to form the **2f** is not clear.
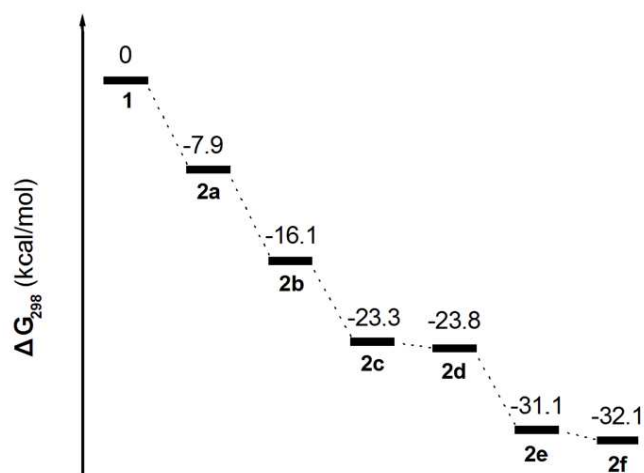

Scheme 3. Potential energy surface for **1** and **2**. (Gaussian 03W (B3LYP/6–31G* basis set))

To disclose the bromination mechanism of **1**, the deitnsity functional theory (DFT) calculations DFT-calculated (B3LYP/6-31G* basis set) were carried out using the Gaussian 03 software package for investigating the potential-energy surface of each bromopyrene derivative in Scheme 3. B3LYP functional was chosen. The geometric structures of bromo-substituted compounds **2** are optimized at 6-31G* level and their parameters were given in supporting information. The frequency and the electronic distribution of **2** were further tested, the results show that the vibration frequency of 2 are with positive value, without imaginary frequency, indicate the calculation of molecular structure energy is the minimum and stable. The relative free energy (ΔG_{298}) is exergonic by 7.9 kcal/mol in the process of bromination of **1**, leading to **2a**, which can be further bromination to afford **2b** and **2c** with an exergonic reaction of 8.2 kcal/mol and 15.4 kcal/mol, respectively. when **1** with the bromine reagent leads to **2c** with an exergonic reaction of 23.3 kcal/mol. The subsequent bromination step from **2c** or **2d** to **2e** and **2f** with an exergonic is ≈ 8.8 kcal/mol.

when **1** with the bromine reagent leads to **2c** with an exergonic reaction of 23.3 kcal/mol. The subsequent bromination step from **2c** or **2d** to **2e** and **2f** with an exergonic is ≈ 8.8 kcal/mol.

Comparison of the geometric structures of **2**, that show that the angle of bromine atom in 6-position of **2c** (∠Br3-C5-C6 = 115.5°) or

8-position of **2e** ($\angle$Br4-C8-C7 = 115.7°), which is less than in other bromo substituted-position (for example: $\angle$Br1-C1-C2 = 120.6 in **2a**). And the *tert*-butyl group located at 7-position of pyrene core have slightly crowded in **2c** and **2e** with angle of 125.7° ± 0.1, which is larger than those in **1** and **2a–b**, **2d** and **2f**. Interesting thing is that **2c** or **2d** was generated from **2b** with similar exergonic (7.2 kcal/mol for **2c** and 7.7 kcal/mol for **2d**). However, the **2d** can not observed by bromination **2b** with an excess of bromine without iron powder presenting in our experiment. In fact, in the presence of iron (III) bromide, **2a–c** and **2e** was synthesized by undergo Friedel-Crafts-type reactions from **1** with bromine. From Scheme 3, the presence of iron (III) bromide might be contribute to lower the activation energy of bromination and induce intramolecular bromine rearrangement in the process of **2d** and **2f**, that bromine atom would shift from active site (6- or 8-position) to K-region (5- or 9-position).
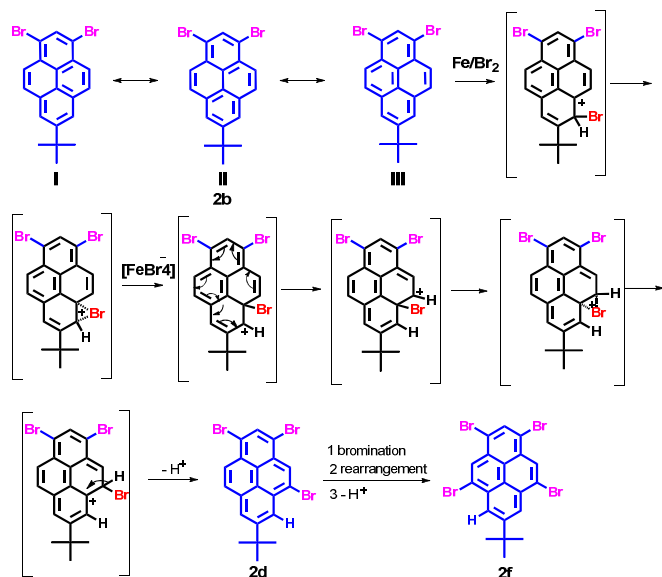

Scheme 4. Possible regioselective bromination mechanism of **1**

The possible bromination reaction pathway has been summarized in Scheme 4. Firstly, The relatively easy electrophilic substitution at the ortho-position to a *tert*-butyl group (6- or 8-position) on the pyrene ring is remarkable because usually the steric bulkiness of a *tert*-butyl group might be expected to direct the substitution towards other positions of the pyrene ring.[7,8] This result is strongly attributable to the high reactivity of the 1-, 3-, 6- and 8-positions of the pyrene ring. Second, however, the pyrene exhibit special electronic structure that the Kekulé structure (I, II and III) show the greatest number of benzenoid rings should have the greatest weight in the superposition diagram, meanwhile, also show the greatest number of double bonds in the "exposed" position have the greatest weight (see supporting information).[26] So, when the bromide attracted the 6-position of **2b**, due to the steric strain involving the *tert*-butyl group and lowing the Gibbs free energy, the bromide would rearrange to 5-position under FeBr$_3$-catalyzed and afford **2c**. Similarly, the tetrabromide **2f** was obtained by the same FeBr$_3$-catalyzed rearrangement in the bromination of tribromopyrenes **2c** and **2d** in the presence of iron powder. The above results strongly

suggest that compounds **2c**, **2d** and **2e** were the intermediates for the formation of the 1,3,5,9-tetrabromo-7-*tert*-butylpyrene **2f**.

In this reaction, Iron powder leads to titled products where bromine is directed to the K-region (positions 5- and 9-) instead of the more reactive positions 6- and 8-. There are two reasons can explain this phenomenon of FeBr$_3$-induced intramolecular bromine rearrangement: one possible reason is a release of steric hindrance is indicated as the driven force for this rearrangement, which is also possible in the absence of FeBr$_3$ where no rearrangement is observed. Another possible reason from DFT-calculation is lowing the activation energy of the rearrangement induced by FeBr$_3$.
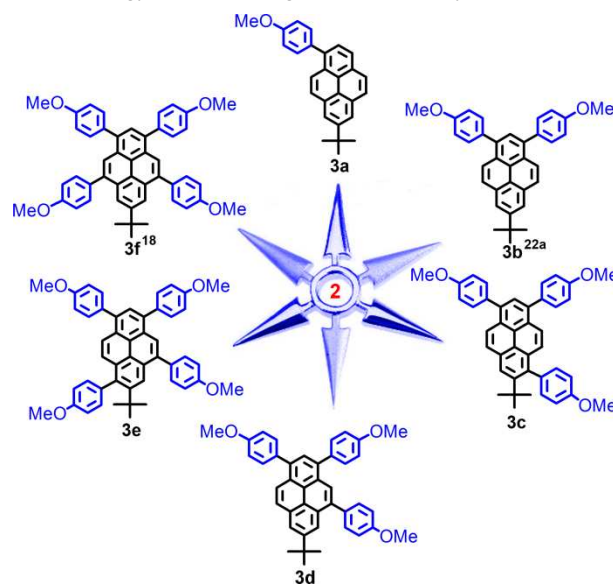
Scheme 5. Synthetic route for compound **3** via a Suzuki-Miyaura cross-coupling reaction, reagents and conditions: a) 4-methoxylphenylboronic acid, [Pd(PPh$_3$)$_4$], Na$_2$CO$_3$, toluene/EtOH, 24 h, 90 °C.

In order to further investigate bromo-substitution positions of the pyrene in more detail, a series of aryl-substituted pyrenes (**3**) were prepared from the resultant bromopyrenes using 4-methoxyphenylboronic acid via a Pd-catalyzed cross-coupling reaction. Using the 4-methoxylphenyl group as an effective substituent, several different shaped pyrenes **3** were synthesized and are displayed in Scheme 5: 7-*tert*-butyl-1-(4-methoxyphenyl)pyrene (**3a**), 7-*tert*-butyl-1,3-bis(4-methoxyphenyl) pyrene (**3b**),[22a] 7-*tert*-butyl-1,3,6-tris(4-methoxyphenyl)pyrene (**3c**), 7-*tert*-butyl-1,3,5-tris-(4-methoxylphenyl)pyrene (**3d**), 7-*tert*-butyl-1,3,5,8-tetrakis(4-methoxyphenyl)pyrene (**3e**) and 7-*tert*-butyl-1,3,5,9-tetrakis(4-methoxyl)phenylpyrene (**3f**)[18]. The molecular structure of all compounds was characterized by their ^{1}H/^{13}C NMR spectra, single-crystal X-ray diffraction, FT-IR spectroscopy, mass spectrometry, as well as by elemental analysis. All analysis results herein on the aryl-substituted pyrene **3** strongly supported our previous predictions.

The performance of the organic compounds in optoelectronic devices strongly relies on the molecular packing and intra/intermolecular interactions in the solid-state. Therefore, investigating the effects of a structure-property relationship between the substituent groups on the pyrene-core using crystal structure and photophysical properties is significant for organic electroluminescence materials. Herein, we expected that the

integration of poly-methoxylphenyl groups with the pyrene core in a molecular structure might influence the crystal packing, leading to favourable optical features and charge-transport properties that could be useful in optoelectronic devices.

Description of crystal structures

Previously, we reported that several Y-shaped aryl-substituted pyrenes with electron-donating/withdrawing groups at the *para*-position of the C_6H_4 rings inefficiently impact on the molecular packing in the solid-state.[22a] Konishi et al. have validated that alkyl groups located at the 1-, 3-, 6-, and/or 8-positions of the pyrene ring play significant roles in tuning the photophysical properties.[15] Herein, this article presents a series of position-substituted pyrenes that not only take place of the active sites (1-, 3-, 6- and 8-positions) but also the K-region (4- and 9-positions) of pyrene, and allow us to shed light on the effect of multiple 4-methoxylphenyl groups on the molecular packing and optical physical properties.
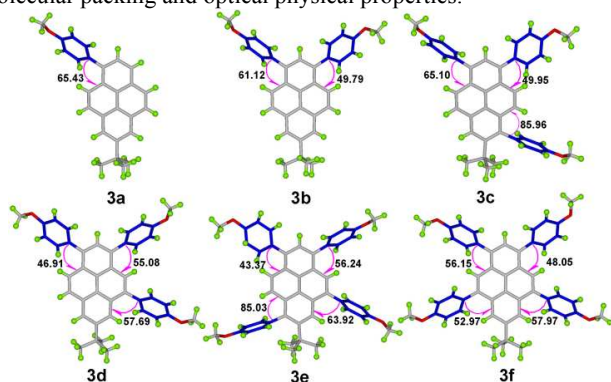
Figure 1. X-ray structures of compounds **3**.

Crystals of **3** suitable for X-ray structure analysis were grown from mixed solvents via slow evaporation at room temperature. And the key crystallographic data are summarized in supporting information Table S2; the crystal structures of molecules for **3** are shown in Figure 1.
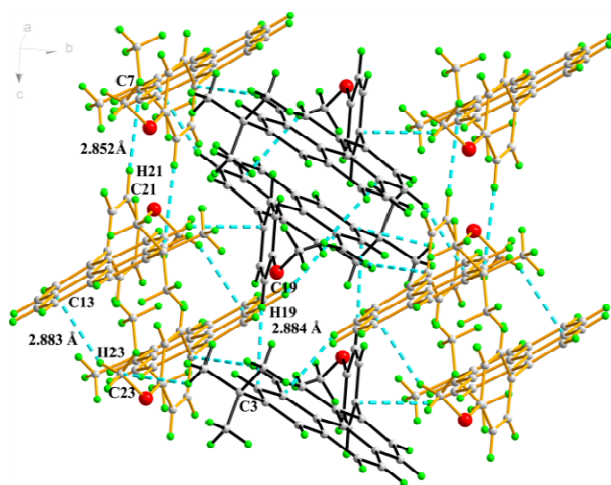

Figure 2. Crystal packing of **3a** by C-H⋯π interactions

Colourless crystals of compound **3a** suitable for X-ray crystallographic analysis were obtained by crystallization from a

mixture of dichloromethane and hexane (1:2, v/v). The single-crystal X-ray structure is depicted in Figure 2. It can be seen that the 4-methoxyphenyl groups in this molecule form a torsion angle (65.43 (17)°) with the plane of the central pyrene ring to prevent face-to-face π-stacking and steric clashes between ortho H atoms on the phenyl ring and those at the 3- and 9-positions. An interesting feature of the compound in the solid-state is that there is an intermolecular C–H⋯π interaction (C19–H19⋯C3 = 2.88 Å, C21–H21⋯C7 = 2.85 Å, C23–H23⋯C13 = 2.88 Å) between neighbouring molecules. These interactions led to a comparatively large twist angle between the pyrene core and the methoxylphenyl fragment, and effectively suppress the formation of the π-π stacking.

On increasing the numbers of 4-methoxylphenyl groups and substituting at different positions in the pyrene derivatives **3a→f**, the space groups (orthorhombic for **3a**, monoclinic for **3b**, **3c** and **3e**, triclinic for **3d** and **3f**) became more asymmetric. It can be seen that the torsional angles between the 4-methoxyphenyl group and the pyrene core decreased from 65.43 (17)° to 48.08 (18)°. With the number of substituted group increasing, the conformation molecules trend for increasing co-planarity.[27] However, without the *tert*-butyl group located at the nodal planes involving the 2-/7-positions in 1,3,6,8-tetrakis(4-methoxyphenyl)pyrene (**4**),[18] the torsion angle is unexpectedly larger than **3** and is up to 76.1 (4)°.
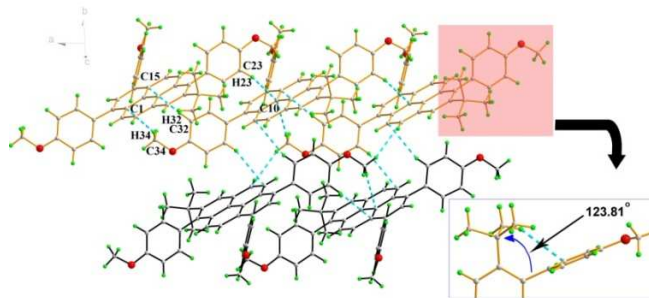

Figure 3. Crystal packing in **3c** by C–H⋯π interactions

Colourless rod crystals of **3c** suitable for X-ray diffraction were recrystallization from a mixture of dichloromethane and methanol by slow evaporation at room temperature. Figure 3 shows the crystal packing in **3c**. The crystal structure revealed the novel asymmetric substitution of the pyrene core. As expected, the 4-methoxyphenyl group successfully substituted at the 6-position of the pyrene with anapproximately perpendicular torsion angle of 88.58(4)°. In the crowded region at the 6- and 7-positions two bulky moieties were introduced, which contact each other by steric interaction. This causes two-fold *tert*-butyl group disorder with occupancy ratio 0.634 (12):0.366 (12) for C18, C19 and C20 and an intramolecular short contact (C18–H18B⋯C26 = 2.81 Å) and significant distortion for the Csp^2 hybridization with an angle of 123.81(15)° at C4–C5–C17. In the off-set packing system of **3c**, the two proximal pyrene molecular planes have a long centroid-centroid distance of 7.97 Å and no π⋯π stacking was observed. The adjacent molecules interacted by a classical C–H⋯π bond (C34–H34⋯C1 = 2.84 Å, C32–H32⋯C15 = 2.82 Å, C23–H23⋯C10 = 2.84 Å). It seems that the close proximity of the 4-methoxyphenyl moiety and the *tert*-butyl group caused strong intermolecular steric hindrance in this packing system.

Table 2. The photophysical and electrochemical properties of compounds **3**, **4** and **5**.

Compounds	λ_{max}abs (nm) Solns[a]/films[b]		λ_{max} PL (nm) Solns[a]/ films[b]		Φ_f[c] solns/films	HOMO (eV)	Energy gap (eV)	τ (ns)[a]	T_m[g]/T_d[h] (°C)
3a	347	nd	391, 407	nd	0.41 / nd	−5.06[d] / nd	3.65^d (3.30)[f]	8.6	141 / 282
3b	363	372	402	450	0.56 / 0.58	−4.93 / −5.44[e]	3.51 (3.17)	8.9	167 / 173
3c	363, 375	381	406	471	0.71 / 0.28	−4.84 / −5.06	3.46 (3.13)	5.2	249 / nd
3e	381	388	420	441	0.76 / 0.58	−4.76 / −5.36	3.37 (3.03)	2.2	240 / 399
3f	379	369	421	443	0.90 / 0.72	−4.76 / −5.37	3.40 (3.03)	5.8	330 / 410
4	391	405	434	488	0.94 / nd	−4.71 / nd	3.24 (2.94)	1.9	271 / nd
5	343, 356	357	411, 433	414	0.24 / 0.17	−4.93 / nd	3.70 (3.31)	18.8	nd / 433

[a] Measured in dichloromethane at room temperature. [b] Measured in thin films. [c] Measured in dichloromethane and in thin films, respectively. [d] Calculation by DFT (B3LYP/6–31G*). [e] Calculated from Onset of first oxidation potential according to equations: -(4.8+E_{ox}^{onset}) [f] Estimated from UV-vis absorption spectra in solution. [g] Melting temperature (T_m) obtained from differential scanning calorimetry (DSC) measurement. [h] Decomposition temperature (T_d) obtained from thermogravimetric analysis (TGA). nd. No determination.

Yellow needles of **3d** were obtained from a mixed solution of dichloromethane/hexane = 1:1; the asymmetric unit of compound **3d** contains one molecule (Figure 4). The molecule exhibits a non-planar and the central pyrene ring has a slight bend; possibly arising from the imbalance of the electrostatic potential on the molecular surface.[27] The inter-planar angles between the central pyrene coreand the outer substituent phenyl rings range from 44.2(5)° to 57.7(5)°. The crystal structure was arranged in columns along the aaxis, through essentially parallel, or near-parallel interactions between translationally equivalent molecules. Each molecule is interlaced with adjacent columns along the a-axis by the formation of π–π stacking with a centroid-to-centroid distance of 4.07 Å and inter-planar angle of 0°. There are numerous C–H···π interactions formed between phenyl hydrogens and neighbouring aromatic rings.
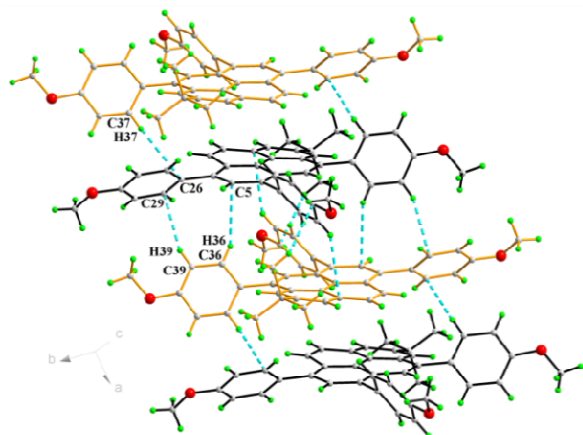
Figure 4. Crystal packing in **3d** by C–H···π interactions

Compound **3e** was dissolved in CHCl$_3$ and kept in a CH$_3$OH atmosphere at room temperature to afford orange single crystals suitable for X-ray diffraction. The crystal system of **3e** is monoclinic with space group P2$_1$/c and is shown in Figure 5. A similar arrangement pattern to **3d** was observed. The molecules also adopt aslipped face-to-face and π–π stacking pattern along the b-axis with acentroid-to-centroid distance of 4.96 Å. This is longer than that observed in **3d**, arising from an extra 4-methoxyphenyl moiety playing a role to prevent the neighbouring molecules getting too

close to each other. Also, the 4-methoxyphenyl group and bulky *tert*-butyl group share a crowded space at the 1- and 2-positions of the pyrene, and these sterics result in the Csp^2 hybridization angle C4–C5–C17 changing to 124.07(6)° via intramolecular hydrogen bonds (C19–H19B···C26 = 2.56 Å, C18–H18B···C22 = 2.53 Å).
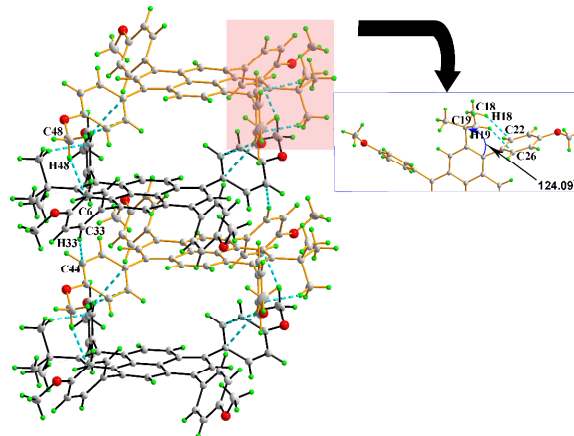
Figure 5. (a) Crystal packing in **3e** by C–H···π interactions

Comparison of tetra-substituted pyrenes **3e**, **3f** and 1,3,6,8-tetrakis(4-methoxyphenyl)pyrene (**4**), the crystal packing in the solid-state is different attribute to the position-substituted diversification.[18,28] For the packing structures of **3a** to **3f**, the X-ray diffraction revealed that the torsion angle decreased between the substituent group and the pyrene core as well as the molecular packing varied significantly from 3D (column structure) to 2D (planar structure) with the number of 4-methoxylpehnyl groups increased. As mentioned above, the number of substituent groups and their positions, as well as the bulky *tert*-butyl groups play an important role in arranging the molecular conformations. The structures became more planar, which in turn was beneficial for π-conjugation and improved the optical density, leading to strong FL emission in the solid-state.[29] In the next section, we discuss the resulting photophysical properties resulting from the presence of multiple 4-methoxylphenyl substituents.

Photophysical properties

The normalized UV-vis absorption and fluorescence spectra for **3** recorded in dichloromethane are shown in Figure 6, For comparision, 1,3,6,8-tetrakis(4-methoxyphenyl)pyrene (**4**)[18] and 2-*tert*-butyl-4,5,7,9,10-pentakis(4-methoxyphenyl)pyrene (**5**)[17a] were also summarized in here for investigating the effect of the positions-dependent aryl-functionalized pyrene derivatives for the packing structures and photophysical properties, and the corresponding photophysical data is summarized in Table 2. Except for **3c** and **5**, all molecules exhibited very similar photophysical characteristics with well-resolved spectral bands in both the shortwavelength of 283−305 nm and long wavelength of 347–391 nm regions. The absorption spectra of **3**→**4** show a maximum band at 347 nm for **3a**, 363 nm for **3b**, 363 nm for **3d**, 381 nm for **3e**, 381nm for **3f** and 391 nm for **4**. However, **3c** has two absorption peaks centered at 295 nm and 375 nm with a shoulder peak at 363 nm; similarly, **5** displays two maxiumn absorption peaks at 296 nm and 356 nm with a shoulder peak at 343 nm. Clearly, both the number of substituents and the substitution position (pathway) strongly influence the electronic absorption;[2] the absorption maximum of **3** revealed a remarkable red-shift. It is thought that such phenomena arise from the increasing number of peripheral arms in this series, which extend the π-conjugation of the pyrenes.
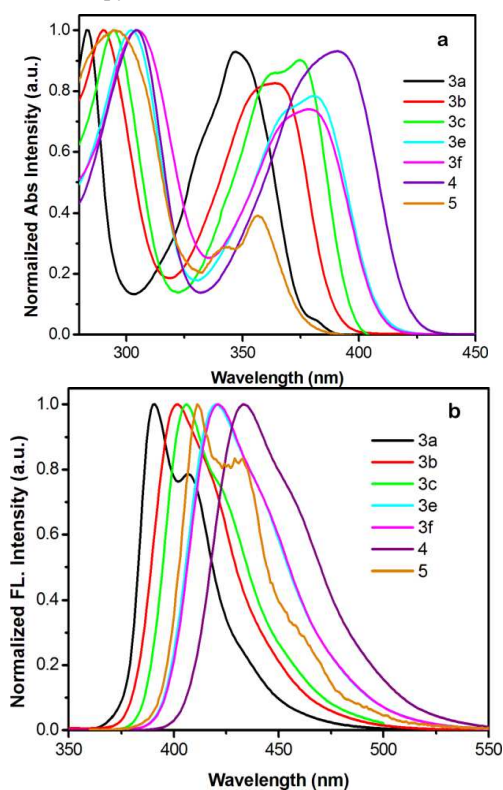
a significant red-shift in comparison with those of the tetrasubstituted derivatives **3e** and **3f**, which is probably a result of the nodal planes passing through the 2,7-positions, leading to a lower electronic density by the rotation of 4-methoxyphenyl group located at 7-position of pyrene core. This suggests the 2,7-substitutions have a small influence on the electronic interaction,[2] and the results have also been reinforced by DFT calculations (mentioned below).

For the emission spectra, all compounds exhibit intense emissions in the blue region (391–434 nm). The emission maxima of **3** and **4** are bathochromically shifted depending on the numbers of 4-methoxylphenyl units, revealing an identical trend to their absorption spectra. No characteristic excimer fluorescence was observed in any of the spectra. It is worth noting that 1,3,5,8-functionalized pyrene **3e** exhibits an emission with λ_{em} values of 420 nm, which almost overlaps with the emission spectrum (421 nm) of 1,3,5,9-functionalized pyrene (**3f**). In general, the substitution pattern of the pyrene moiety has a substantial effect on the fluorescence wavelength, and the effect of being substituted at the active 1-, 3-, 6- and 8-positions for the $S_1 \leftarrow S_0$ excitations is more significant than at the K-region (4-, 5-, 9- and 10-positions).[2]

In the case of **3e** and **3f**, smaller red-shifts in their electronic absorption profiles indicate that the structural changes and/or electronic distribution changes can cause an electronic communication missing in the pyrene cores.[30] For **5**, a deep-blue emission was observed with a maximum peak at 411 nm and a shoulder at 430 nm in solution.

Figure 6. (a) Normalized UV-vis absorption and (b) emission spectra of compounds **3**, **4** and **5** recorded in dichloromethane at ca. ∼10^{-5}–10^{-6} M at 25 °C.

The longest absorption (λ_{max}) exhibited by **3e** and **3f** was approximately red shifted by ca. 34 nm versus **3a**, indicating the HOMO−LUMO energy gap of **3** decreased on increasing the conjugation length. Interestingly, for the hand-shaped compound **5**, despite it having the most substituents, the absorption does not show
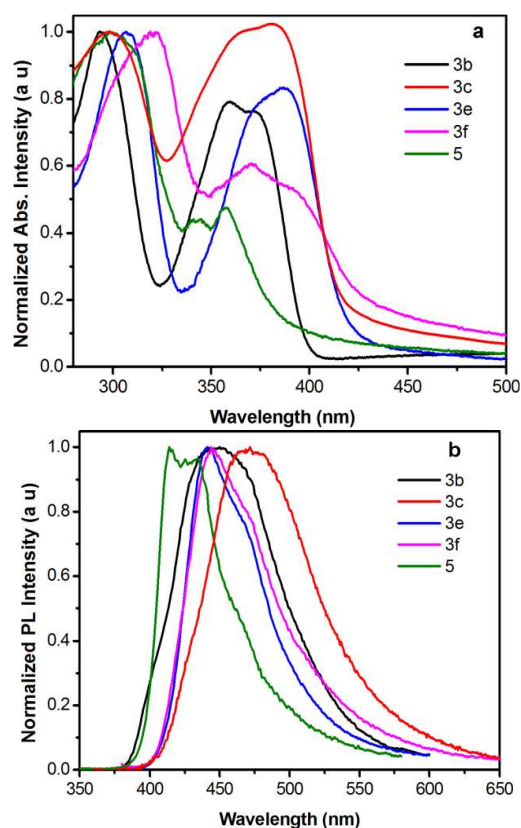

Figure 7. (a) Normalized UV-vis absorption and (b) emission spectra of **3** and **5** in thin films.

The UV-vis absorption and emission spectra of selected pyrenes in the solid-state are shown in Figure 7, and the optical data are summarized in Table 2. Compared with the corresponding solutions, the absorption for **3b**, **3c**, **3e**, **4** and **5** films reveals a slight red-shift (about 10 nm) (Table 2). However, the absorption of **3f** as a film shows a slight blue-shift in comparison with that in solution. This unusual blue-shift might be due to the different dielectric constant.[31] The emission maxima of **3b**, **3e** and **3f** as thin films exhibited red-shifts of less than 48 nm relative to those in solution, and the compound **3c** exhibits a red-shift of 65 nm (from 406 nm to 471 nm). (Table 2). On increasing the numbers of 4-methoxylphenyl moieties, the red-shift decreased in the following order: **5** (3 nm) < **3f** (22 nm) ≈ **3e** (21 nm) < **3b** (48 nm) < **4** (54 nm) < **3c** (65 nm), indicating the positions-substitution of aryl-functionalized would influence the electronic interaction. Owing to the strong intermolecular interactions in the thin film of **3c** and **4**, the emission maxima exhibited a greater red-shift as a thin film state with high noise level.[32]

Different to the 1,3,6,8-tetrakis(4-methoxyphenyl)pyrene **4**,[18] that tends to exhibit a high noise level PL spectrum in the solid-state. the tetra-substituted pyrenes **3e** and **3f** exhibited clear and sharp emission peaks in the blue-region without extra excimer emissions in the solid-state owing to the bulky *tert*-butyl group located at 7-position of the pyrene ring suppressing the aggregation. Compound **4** also presents a very high fluorescence quantum yield (Φ_f^c) of the range of ~0.94 in solution.

For comparison, the quantum yields of **3b**, **3c**, **3e** and **3f** in the solid-state were also investigated (0.58 for **3b**, 0.28 for **3c**, 0.58 for **3e** and 0.72 for **3f**). However, for **5**, low fluorescence quantum yields in both solution and the solid-state were obtained due to energy loss that is likely occurring during the exciton migration.[33] The fluorescence lifetime of **3a-c**, **3e**, **3f**, **4** and **5** are 8.6 ns, 8.9 ns, 5.2 ns, 2.2 ns, 5.8 ns, 1.9 ns, 18.8 ns, respectively. Excellent optical features were obtained in these compounds, which make them of potential use in new optoelectronic devices, such as blue emitters in OLEDs, or as models for further exploring a new generation of organic materials based on pyrene.

Quantum chemistry computation

To gain further insight into the effect of multi-substituents and pathways on the electronic structure and spectral properties of compounds **3**, **4** and **5**, quantum chemical calculations were calculated using DFT methods at the B3LYP/6–31G* level. The calculated energies of the frontier molecular orbitals are presented in Figure 8 and in the supporting information.

Scrutiny of the electronic structures reveals that both HOMOs and LUMOs of **3** were primarily delocalized over the entire pyrene component, as well as slightly in the peripheral phenyl moiety, the only difference being in the energy of these frontier molecular orbitals, which in turn relied on the system architecture. For instance, on increasing of the numbers of the substituents from **3a** to **3f**, the HOMO values are more posotive varied from −5.06 eV (**3a**) to −4.76 (**3f**) eV, the increased positions-dependent substitution resulted in a lowering of both the HOMOs and LUMO by 0.3 eV and 0.05 eV, respectively. Obviously, The effects of multiple substituents is

greater for the HOMOs than for the LUMOs with a sizable shrinking of the HOMO−LUMO gap by 0.28 eV with respect to **3a**, which is in good agreement with the experimentally measured results in tendency, the slight different to those obtained by UV-vis absorption ($\Delta E_{\text{gap opt}}$ = 0.27 eV) owing to the DFT-calculation was performed in the gas phase.
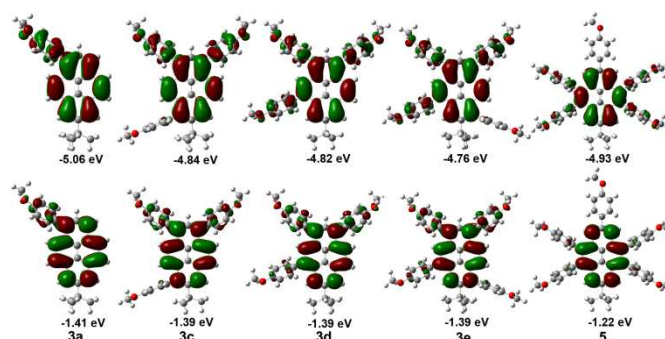

Figure 8. Computed molecular orbital plots (B3LYP/6–31G*) of compounds of **3** and **5**; the upper plots represent the HOMOs, and the lower plots represent the LUMOs.

Compared with **3e**/**3f** and **4**, the presence of the *tert*-butyl group at the 7-position, could lead to a lower energy gap by lowing the molecular LUMOs. With the number of substituent groups increased, from the mono-substituted **3a** to the tetra-substituted pyrenes **4** and **3e**/**3f**, the energy gap of the representative molecules decreased. Especially, the speical electronic structure of penta-substituted pyrene **5** inhibits absorption spectra is different from others, due to the substituted group at the K-region (4,5,9,10-positions) in favour of blue-shift by the improving energy gap of the molecular structure; when as the 4-methoxyphenyl group located at nodal planes would weak electronic coupling with entire pyrene,[4] attributing to little influence on $S_2 \leftarrow S_0$ absorption but lager influence on $S_1 \leftarrow S_0$ absorption.[34] So, These conclusions are also consistent with our quantum chemical calculations.

Electrochemistry

The electrochemical properties of selected compounds **3** were investigated in CH_2Cl_2 solution by cyclic voltammetry (CV) in a three-electrode electrochemical cell with Bu_4NClO_4 (0.1 M) and Ag/AgCl as electrolyte and reference electrode respectively, and using ferrocene (Fc/Fc$^+$) as the internal standard with a scan rate of 100 mVs^{-1} at room temperature.

As shown in Figure 9, compound **3b** exhibits a quasi-reversible oxidation processin the positive potential region with a oxidation process around 1.0 V (vs. Ag/AgCl), and compounds **3c**, **3e** and **3f** exhibit two reversible or quasi-reversible oxidation processes, respectively. On the basis of the absorption spectra and the CV, the corresponding HOMO and LUMO energy levels were confirmed and the results are displayed in Table 3 and in the supporting information (Table S3). The HOMO values were calculated from the oxidation potential by the empirical formulae HOMO = −(4.8+$E_{\text{ox}}^{\text{onset}}$), where E_{ox} is the onset of the oxidation potential. The HOMO values were −5.44 eV for **3b**, −5.06 eV for **3c**, −5.35 eV for **3e** and −5.36 eV for **3f**. The LUMO levels were determined from the HOMO and energy gap.

For **3b** and **3c** containing increasing numbers of 4-methoxyphenyl moieties in different positions on the pyrene, similar energy gap (3.17 eV for **3b** and 3.13 eV for **3c**) with different HOMO and LUMO levels are achieved.
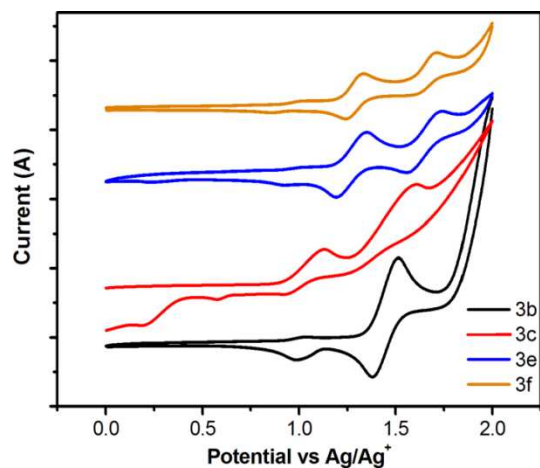

Figure 9. Cyclic voltammograms recorded for selected compounds **3**.

Additionally, **3e** and **3f** have same numbers of substituents but different substituted position, that also showed similar HOMO (–5.36 eV for **3e** and –5.37 eV for **3f**, respectively) and LUMO (–2.33 eV for **3e** and –2.34 eV for **3f**, respectively). From both Figure 9 and Table S2, it can be seen that oxidation potential are shifted to more positive values when increasing the number of substituents. The half-wave potentials for compounds **3b** (2 substituents), **3c** (3 substituents), **3e** (4 substituents) and **3f** (4 substituents) are 1.45 eV, 1.51 eV, 1.64 eV and 1.67 eV, respectively. Furthermore, the reduction potentials was effected dependent on position, and substituted at active sites of 1,3,6,8-position would lower LUMO level and K-region of 4,5,9,10-position contributes to improve LUMO level.

Conclusions

In summary, the bromination mechanism of pyrene was explored by experimental methods. Clear evidence was observed for theformation of mono- to tetrakis(4-methoxyphenyl)-substituted pyrenes (**3**), which were synthesized by Suzuki-Miyaura cross-coupling reaction of the corresponding bromopyrenes with 4-methoxyphenyl boronic acid, and characterized by single-crystal X-ray diffraction, ^{1}H/^{13}C NMR spectra, mass spectrometry as well as elemental analysis. These results supported our conclusions on the bromination mechanism, namely that it was possible to regioselectively generate the mono- to tetrabromopyrenes from the 2-*tert*-butylpyrene (**1**) via a stepwise electrophilic substitution using a FeBr$_3$-catalyzed rearrangement. Otherwise, the spectroscopic data, DFT calculations and electron chemistry results of the aryl-functionalized pyrenes indicate that the HOMOs and LUMOs level can be tuned by both the number of substitution and substutited-position cooperativity; the numbers of substituent moieties contribute to higher oxidation potential and the reduction potential was attributed to position-substituted. The series of new molecular materials combines excellent optical features with reasonable

thermal stabilities, making such molecules potential candidates in optoelectronic applications such as OLED-like devices. Further investigations on their usefulness in organic electroluminescent devices are in progress in our laboratory.

Experimental Section

Materials: Unless otherwise stated, all other reagents used were purchased from commercial sources and used without further purification. The preparations of 2-*tert*-butylpyrene (**1**)[35] was reported previously.

All melting points (Yanagimoto MP-S$_1$) are uncorrected. ^{1}H/^{13}C NMR spectra (300 MHz) were recorded on a Nippon Denshi JEOL FT-300 NMR spectrometer. IR spectra were measured for samples as KBr pellets in a Nippon Denshi JIR-AQ2OM spectrophotometer. Mass spectra were obtained with a Nippon Denshi JMS-HX110A Ultrahigh Performance Mass Spectrometer at 75 eV using a direct-inlet system. Elemental analyses were performed by Yanaco MT-5. UV/ Vis spectra were obtained with a Perkin–Elmer Lambda 19 UV/Vis/NIR spectrometer in various organic solvents. Fluorescence spectroscopic studies were performed in various organic solvents in a semimicro fluorescence cell (Hellma®, 104F-QS, 10 × 4 mm, 1400 µL) with a Varian Cary Eclipse spectrophotometer. Fluorescence quantum yields were measured using absolute methods. Thermogravimetric analysis (TGA) was undertaken using a SEIKO EXSTAR 6000 TG/ DTA 6200 unit under nitrogen atmosphere at a heating rate of 10 °C min^{-1}. Differential scanning calorimeter (DSC) was performed using a Perkin–Elmer Diamond DSC Pyris instrument under nitrogen atmosphere at a heating rate of 10 °C min^{-1}. Photoluminescence spectra were obtained using a FluroMax-2 (Jobin-Yvon-Spex) luminescence spectrometer. Electrochemical properties of HOMO and LUMO energy levels were determined by Electrochemical Analyzer. The quantum chemistry calculation was performed on the Gaussian 03W (B3LYP/6–31G* basis set) software package.[36]

Synthesis of 2-*tert*-butylpyrene (1). A mixture of pyrene (5 g, 24.2 mmol) and 2-chloro-2-methylpropane (2.62 g, 3.23 mL) was added in 40 mL of CH$_2$Cl$_2$ at 0 °C and stirred for 15 min. Powdered anhydrous AlCl$_3$ (3.62 g, 27.2 mmol) was slowly added to a stirred solution. The reaction mixture was continuously stirred for 3 h at 28 °C and the reaction process was tracked by GC, then poured into a large excess of ice/water. The reaction mixture was extracted with CH$_2$Cl$_2$ (2 × 50 mL). The combined organic extracts were washed with water and brine, dried with anhydrous MgSO$_4$ and evaporated. The residue was crystallized from hexane to afford pure 2-*tert*-butylpyrene (**2**) in 71% yield (4.56 g) as a gray powder. Recrystallization from hexane gave **2** as colourless prisms. Mp: 111.5–113.2 °C (lit.[35] Mp: 110–112 °C). The ^{1}H NMR spectrum agreed with the reported values. ^{1}H NMR (300 MHz, CDCl$_3$): δ (TMS, ppm) 1.59 (s, 9H, *t*Bu), 8.18 (d, J = 9.2 Hz, 2H, pyrene-*H*), 8.30 (s, 2H, pyrene-*H*), 8.37 (d, J = 9.2 Hz, 2H, pyrene-*H*), 8.47 (s, 1H, pyrene-*H*).

Synthesis of 1-bromo-7-*tert*-butylpyrene (2a).
Run 1: Lewis acid-catalysed bromination of 2-*tert*-butylpyrene
A mixture of 2-*tert*-butylpyrene (**1**) (0.26 g, 1 mmol) and iron powder (0.56 g, 10 mmol) were combined in CH$_2$Cl$_2$ (10 mL) at

0 °C with stirring for 30 min. A solution of Br_2 (0.051 mL, 1 mmol) in CH_2Cl_2 (10 mL) was slowly added drop-wise with vigorous stirring. After this addition, the reaction mixture was continuously stirred for 5 h at 28 °C. The mixture was quenched with $Na_2S_2O_3$ (10%) and extracted with CH_2Cl_2 (20 mL × 2). The combined organic extracts were washed with water and brine and evaporated. The crude product was a brown colour, and the residue was recrystallized from a mixted solution of toluene-hexane (1:2) to give pure 1-bromo-7-*tert*-butylpyrene (**2a**) in 83% yield (290 mg) as a white powder.

Run 2: A solution of benzyltrimethylammonium tribromide (BMTABr$_3$) (7.57 g, 19.4 mmol) in dry CH_2Cl_2 (50 mL) was slowly added to a solution of 2-*tert*-butylpyrene (**1**) (5 g, 19.4 mmol) in dry CH_2Cl_2 (150 mL) at 0 °C under a nitrogen atmosphere. The resulting mixture was allowed to slowly warm up to 28 °C and stirred overnight. The reaction mixture was quenched with $Na_2S_2O_3$ and extracted with CH_2Cl_2 (2 × 50 mL). The combined organic extracts were dried with anhydrous $MgSO_4$ and evaporated. The residue was crystallized from hexane to give pure 1-bromo-7-*tert*-butylpyrene (**2a**) in 84% yield (5.5 g) as white crystals. The ^{1}H NMR spectrum completely agreed with the reported values.[22b] ^{1}H NMR (300 MHz, CDCl$_3$): δ (TMS, ppm) 1.59 (s, 9H, *t*Bu), 7.99 (d, *J* = 8.2 Hz, 1H), 8.01 (d, *J* = 8.79 Hz, 1H), 8.08 (d, *J* = 9.0 Hz, 1H), 8.17 (d, *J* = 10 Hz, 1H), 8.20 (d, *J* = 8.22 Hz, 1H), 8.27–8.27 (m, 2H), 8.40 (d, *J* = 9.0 Hz, 1H). FAB-HRMS: *m/z* calcd. for $C_{20}H_{17}Br$ 337.3; found 335.9 [M$^+$]. Anal. Calcd for $C_{20}H_{17}Br$: C, 71.23; H, 5.08; found: C, 72.25; H, 6.33.

Synthesis of 1,3-dibromo-7-*tert*-butyl-pyrene (2b)

Run 3: A mixture of 2-*tert*-butylpyrene (**1**) (0.26 g, 1 mmol) and iron powder (0.56 g, 10 mmol) were added in CH_2Cl_2 (10 mL) at 0 °C with stirring for 30 min. A solution of Br_2 (0.105 mL, 2 mmol) in CH_2Cl_2 (10 mL) was slowly added drop-wise with vigorous stirring. After this addition, the reaction mixture was continuously stirred for 5 h at 28 °C. The mixture was quenched with $Na_2S_2O_3$ (10%) and extracted with CH_2Cl_2 (20 mL × 2). The combined organic extracts were washed with water and brine and evaporated. The crude product was black in colour. The residue was washed with hot hexane and filtered to afford 1,3-dibromo-7-*tert*-butylpyrene (**2b**) 146 mg (35%). The solution was evaporated and recrystallized from a mixed solution of CH_2Cl_2-hexane (1:2) to give pure 1-bromo-7-*tert*-butylpyrene (**2a**) in 50% yield (170 mg) as white powder.

Run 4: To a mixture of 2-*tert*-butylpyrene (**1**) (2.58 g, 10 mmol) in CH_2Cl_2 (30 mL) was added drop-wise a solution of BTMABr$_3$ (benzyltrimethylammonium tribromide) (13.7 g, 35 mmol) in CH_2Cl_2 (20 mL) at 0 °C for 1 h under an argon atmosphere. The resulting mixture was allowed to slowly warm up to 28 °C and stirred overnight. The reaction mixture was poured into ice-water (60 mL) and neutralized with an aqueous 10% $Na_2S_2O_3$ solution. The solution was extracted with CH_2Cl_2 (2 × 50 mL). The organic layer was washed with water (2 × 20 mL) and saturated brine (20 mL), and then the solution was dried ($MgSO_4$) and condensed under reduced pressure. The crude compound was washed with hot hexane to afford pure 1,3-dibromo-7-*tert*-butylpyrene (**2b**) in 76% yield (3.02 g) as a colourless solid. Recrystallization from hexane gave **2b** as a gray solid, Mp: 199.5–201.2 °C. The ^{1}H NMR spectrum agreed with the reported values.[25] ^{1}H NMR (300 MHz, CDCl$_3$): δ (TMS,

ppm) 1.59 (s, 9H, *t*Bu), 8.15 (d, *J* = 9.2 Hz, 2H, pyrene-*H*), 8.30 (s, 1H, pyrene-*H*), 8.47 (d, *J* = 9.2 Hz, 2H, pyrene-*H*), 8.47 (s, 1H, pyrene-*H*). FAB-HRMS: *m/z* calcd. for $C_{20}H_{16}Br_2$ 416.2; found 417.4 [M$^+$]. Anal. Calcd for $C_{20}H_{16}B_2$: C, 55.72; H, 3.88; found: C, 55.05; H, 4.56.

Run 5: Synthesis of 1,3,6-tribromo-7-*tert*-butylpyrene (2c)[25]

2-*tert*-Butylpyrene (**1**) (1.3 g, 5.03 mmol) was dissolved in CH_2Cl_2 (20 mL) and stirred for 30 min. at 25 °C. To this solution was added Br_2 (1 mL, 19.4 mmol) and violently stirred for 24 h. The reaction mixture was poured into ice-water (50 mL) and neutralized with an aqueous 10% $Na_2S_2O_3$ solution, the mixture was extracted with CH_2Cl_2 (2 × 50 mL), and the organic layer was washed with brine and evaporated. The residue was recrystallized from a mixed solution of CH_2Cl_2-hexane (2:1) to afford 1,3,6-tribromo-7-*tert*-butylpyrene(**2c**) in 65% yield (1.6 g). Mp: 276–277 °C. The ^{1}HNMR spectrum completely agreed with the reported values.[25] ^{1}H NMR (300 MHz, CDCl$_3$): δ (TMS, ppm) 1.81 (s, 9H, *t*Bu), 8.08 (d, *J*= 9.2 Hz, 1H, pyrene-*H*), 8.10 (s, 1H, pyrene-*H*), 8.34 (d, *J* = 8.58Hz, 1H, pyrene-*H*), 8.39 (d, *J* = 9.7 Hz, 1H, pyrene-*H*), 8.46 (s, 1H, pyrene-*H*), 8.85 (d, *J* = 9.7 Hz, 1H, pyrene-*H*). FAB-HRMS: *m/z* calcd. for $C_{20}H_{15}Br_3$ 495.05; found 494.0 [M$^+$]. Anal. Calcd for $C_{20}H_{15}Br_3$: C, 48.52; H, 3.05; found: C, 49.32; H, 4.55.

Run 6: Lewis acid-catalyzed bromination of 2-*tert*-butylpyrene

A mixture of 2-*tert*-butylpyrene (**1**) (0.26 g, 1 mmol) and iron powder (0.56 g, 10 mmol) were added to CH_2Cl_2 (10 mL) at 0 °C with stirring for 30 min. A solution of Br_2 (0.153 mL, 3 mmol) in CH_2Cl_2 (10 mL) was slowly added drop-wise with vigorous stirring. After this addition, the reaction mixture was continuously stirred for 5 h at 28 °C. The mixture was quenched with $Na_2S_2O_3$ (10%) and extracted with CH_2Cl_2 (2 × 20 mL). The combined organic extracts were washed with water and brine and evaporated. The crude product was washed with hot hexane to afford mixture of white compounds **2d** and **2f** (430 mg), the mixture is difficult to separate by common chromatography. The yield was evaluated by ^{1}H NMR spectral analysis (25% for **2d,** 50% for **2f**). The product cannot further been separated by High-speed Counter-current Chromatography (HSCCC) and was used as a mixture for the Suzuki coupling reactions. ^{1}H NMR (300 MHz, CDCl$_3$) for **2d**: δ (TMS, ppm) 1.64 (s, 9H, *t*Bu), 8.79 (s, 2H, pyrene-*H*), 8.86 (d, *J* = 9.8 Hz, 1H, pyrene-*H*), 8.89 (d, *J*= 8.86 Hz, 1H, pyrene-*H*), 8.90 (s, 1H, pyrene-*H*), 8.92 (s, 1H, pyrene-*H*).

Run 7: Synthesis of 1,3,5,9-tetrabromo-7-*tert*-butylpyrene (2f)

A mixture of 2-*tert*-butylpyrene (0.512 g, 2 mmol) and iron powder (0.56 g, 10 mmol) were added to CH_2Cl_2 (10 mL) at 0 °C with stirring for 15 min. A solution of Br_2 (0.61 mL, 12 mmol) in CH_2Cl_2 (15 mmol) was slowly added drop-wise with vigorous stirring. After this addition, the reaction mixture was continuously stirred for 4 h at28 °C. The mixture was quenched with $Na_2S_2O_3$ (10%) and extracted with CH_2Cl_2 (2 × 50 mL). The combined organic extracts we rewashed with water and brine and evaporated. The crude product was gray in color. The crude product was insoluble in common organic solvents such as benzene, hexane, methanol etc. and slightly dissolved in CH_2Cl_2 or CHCl$_3$. The residue was dissolved in hot CHCl$_3$ and filtered, and the product was crystallized from CHCl$_3$ to give pure 1,3,5,9-tetrabromo-7-*tert*-butylpyrene (**2f**) in 84% yield (978 mg) as a white powder. Mp: 303.4–305.0 °C. IR

(KBr): v_{max} (cm^{-1}) = 2962, 2365, 1579, 1523, 1461, 1425, 1392, 1363, 1267,1195, 1132, 1027, 1012, 941, 877, 809, 655, 474. ^{1}H NMR (300MHz, CDCl$_3$): δ (TMS, ppm) 1.65 (s, 9H, tBu), 8.47 (s, 1H, pyrene-H2), 8.71 (s, 2H, pyrene-H), 8.79 (s, 2H, pyrene-H). Due to the poor solubility in organic solvents it was not further characterized by ^{13}C NMR spectroscopy. FAB-HRMS: m/z calcd. for C$_{20}$H$_{14}$Br$_4$ 573.78; found 573.62 [M$^+$]. Anal. Calcd for C$_{20}$H$_{14}$Br$_4$: C, 41.85; H, 2.46;   found: C, 42.05; H, 2.53.

Run 8: Lewis acid-catalysed bromination of 1,3,6-tribromo-7-$tert$- butylpyrene (2c)

A mixture of 1,3,6-tribromo-7-$tert$-butylpyrene (**2c**) (200 mg, 0.4 mmol) and iron powder (100 mg, 1.8 mmol) were added to CH$_2$Cl$_2$ (15 mL) at 0 °C with stirring for 15 min. A solution of Br$_2$ (0.052mL, 1.01 mmol) in CH$_2$Cl$_2$ (5 mL) was slowly added dropwise with vigorous stirring. After this addition, the reaction mixture was continuously stirred for 4 h at 28 °C. The mixture was quenched with Na$_2$S$_2$O$_3$ (10%) and extracted with CH$_2$Cl$_2$ (2 × 20 mL). The combined organic extracts were washed by water and brine and evaporated. The crude product was dried and identified by ^{1}H NMR spectroscopy. The yield was evaluated by ^{1}HNMR at 70% for **2e**, 30% for **2f**. The product was not further separated and used as the mixture for the Suzuki coupling reaction. The greenish-yellow crude product was insoluble in common organic solvents such as benzene, hexane and methanol, and slightly soluble in CH$_2$Cl$_2$ or CHCl$_3$. So the crude product was recrystallized from CHCl$_3$ to afford a small amount of **2e** for ^{1}H NMR spectra analysis, ^{1}H NMR (300 MHz, CDCl$_3$): δ (TMS, ppm) 1.83 (s, 9H, tBu), 8.46 (d, J = 9.5 Hz, 1H, pyrene-H), 8.51 (s, 1H, pyrene-H), 8.76 (s, 1H, pyrene-H), 8.85 (s, 1H, pyrene-H), 8.91 (d, J = 9.9 Hz, 1H, pyrene-H).

Run 9: Lewis acid-catalysed bromination of 2e/2f

A mixture of **2e/2f** (100 mg, 0.17 mmol) and iron powder (50 mg, 0.9 mmol) were added to CH$_2$Cl$_2$ (15 mL) at 0 °C with stirring for 15min. A solution of Br$_2$ (0.025 mL, 0.49 mmol) in CH$_2$Cl$_2$ (5 mL) was slowly added drop-wise with vigorous stirring. After this addition, the reaction mixture was continuously stirred for 8 h at 28 °C. The mixture was quenched with Na$_2$S$_2$O$_3$ (10%) and extracted with CH$_2$Cl$_2$ (2 × 20 mL). The combined organic extracts were washed with water and brine and evaporated. The residue (85 mg) was dried and identified by ^{1}H NMR spectroscopy. The yield was evaluated by ^{1}H NMR spectral analysis (25 % for **2e**, 75 % for **2f**).

Synthesis of 4-methoxylphenyl substituted pyrene derivatives 3

The pyrene derivatives **3** were synthesized from resultant bromopyrenes with 4-methoxylphenylboronic acid by Suzuki-Miyaura cross coupling reaction in good yield. Although the mixture of bromopyrenes, **2d/2f** and **2e/2f** could not be separated, the final products **3d, 3e** and **3f** were isolated by column chromatography without complication.

Synthesis of 7-$tert$-butyl-1-(4-methoxyphenyl)pyrene (3a)

A mixture of 1-bromo-7-$tert$-butylpyrene 2a (400 mg, 1.2 mmol), 4-methoxyphenylboronic acid (303 mg, 2.0 mmol) in toluene (12 mL) and ethanol (4 mL) at room temperature was stirred under argon, and K$_2$CO$_3$ (2 M, 20 mL) solution and Pd(PPh$_3$)$_4$ (70 mg, 0.06 mmol) were added. After the mixture was stirred for 30 min. at room temperature, the mixture was heated to 90 °C for 24 h with stirring. After cooling to room temperature, the mixture was quenched with water, extracted with CH$_2$Cl$_2$ (3 × 10 mL) and washed with water

and brine. The organic extracts were dried with MgSO$_4$ and evaporated. The residue was purified by column chromatography eluting with CH$_2$Cl$_2$-hexane (2:1) to give **3a** as a white solid. Recrystallization from (CH$_2$Cl$_2$-hexane, 1:1) gave 7-$tert$-butyl-1-(4-methoxyphenyl) pyrene (**3a**) in 54% yield (235 mg) as colourless crystals. Mp: 141.2–143.5 °C. IR (KBr): v_{max} (cm^{-1}) = 2952, 1604, 1520, 1496, 1437, 1246, 1172, 1032, 878, 849, 826, 729, 681, 567, 526, 489. ^{1}H NMR (300 MHz, CDCl$_3$): δ (TMS, ppm) 1.58 (s, 9H, tBu), 3.93 (s, 3H, OMe), 7.10 (d, J = 8.7 Hz, 2H, Ar-H), 7.56 (d, J = 8.7Hz, 2H, Ar-H), 7.92 (d, J = 7.8 Hz, 1H, pyrene-H), 7.99 (d, J = 9 Hz, 1H, pyrene-H), 8.05 (s, 2H, pyrene-H), 8.15 (d, J = 1.8 Hz, 1H, pyrene-H), 8.18 (d, J = 2.4 Hz, 1H, pyrene-H), 8.22 (d, J = 1.8 Hz, 1H, pyrene-H). ^{13}C NMR (100 MHz, CDCl$_3$): δ (TMS, ppm) 158.9, 149.1, 137.2, 133.7, 131.6, 131.3, 130.8, 130.2, 128.4, 127.5, 127.4, 127.29, 127.26, 125.2, 124.9, 124.4, 123.2, 122.3, 122.0, 113.8, 55.4, 35.2, 31.9. FAB-HRMS: m/z calcd. for C$_{27}$H$_{24}$O 364.18; found 364.25 [M$^+$]. Anal. Calcd for C$_{27}$H$_{24}$O: C, 88.97; H, 6.64; found: C, 88.68; H, 6.52.

7-$tert$-Butyl-1,3-bis(4-methoxyphenyl)pyrene (3b) was obtained as yellow prisms (CH$_2$Cl$_2$-hexane, 1:1) (113 mg, 69%). Mp: 167 °C. IR (KBr): v_{max} (cm^{-1}) = 2958, 1610, 1512, 1498, 1456, 1396, 1363, 1286, 1246, 1174, 1039, 877, 835, 727, 660, 607, 580, 553, 418. ^{1}H NMR (300 MHz, CDCl$_3$): δ (TMS, ppm) 1.58 (s, 9 H, pyrene-tBu), 3.93 (s, 6 H, OMe), 7.10 (d, J = 8.8 Hz, 4H, Ar-H), 7.60 (d, J = 8.6 Hz, 4H, Ar-H), 7.91 (s, 1H, pyrene-H), 8.00 (d, J = 9.4 Hz, 2H, pyrene-H), 8.18 (d, J = 9.33 Hz, 2H, pyrene-H), 8.19 (s, 2H, pyrene-H). ^{13}C NMR (75 MHz, CDCl$_3$): δ (TMS, ppm) 159.0, 149.1, 136.8, 133.5, 131.7, 131.2, 129.1, 127.6,127.4, 125.4, 125.2, 123.5, 122.0, 113.8, 55.4, 35.2, 31.9. FAB-HRMS: m/z calcd. for C$_{34}$H$_{30}$O$_2$ 470.22; found 470.2[M$^+$]. Anal. Calcd for C$_{34}$H$_{30}$O$_2$: C, 86.77; H, 6.43; found: C, 86.53; H, 6.41.

7-$tert$-Butyl-1,3,6-tris(4-methoxyphenyl)pyrene (3c) was obtained as yellow, needle-like crystals. (CH$_2$Cl$_2$-hexane, 3:1) (155 mg, 67%). Mp: 249 °C. ^{1}H NMR (300 MHz, CDCl$_3$): δ (TMS, ppm) 1.41 (s, 9 H, pyrene-tBu), 3.86 (s, 3H, OMe), 3.91 (s, 6 H, OMe), 7.00 (d, J = 8.0 Hz, 4H, Ar-H), 7.08 (d, J = 8.4 Hz, 2H, Ar-H), 7.24–7.36 (m, 1H, pyrene-H, 2H, Ar-H), 7.51 (d, J = 8.4 Hz, 2H, Ar-H), 7.58 (d, J = 8.4 Hz, 2H, Ar-H), 7.89 (s, 1H, pyrene-H), 7.97 (d, J = 9.6 Hz, 1H, pyrene-H), 8.00 (d, J = 9.6 Hz, 1H, pyrene-H), 8.18 (d, J = 9.2 Hz, 2H, pyrene-H), 8.37 (s, 1H, pyrene-H). ^{13}C NMR (100 MHz, CDCl$_3$): δ (TMS, ppm) 158.9, 158.88, 158.7, 146.3, 136.8, 136.6, 136.58, 134.1, 133.6, 133.4, 133.1, 132.1, 131.7, 131.6, 130.5, 129.2, 127.9, 127.5, 127.1, 126.0, 125.1, 124.7, 123.4, 123.4, 113.8, 113.7, 112.8, 55.38, 55.36, 55.29, 37.2, 33.1. FAB-HRMS: m/z calcd. For C$_{41}$H$_{36}$O$_3$ 576.27; found 576.34 [M$^+$]. Anal. Calcd for C$_{41}$H$_{36}$O$_3$: C, 85.39; H, 6.29; found: C, 85.53; H, 6.21.

Synthesis of 7-$tert$-butyl-1,3,5-tris(4-methoxyphenyl)pyrene (3d) and 1,3,5,9-tetrakis(4-methoxyphenyl)pyrene (3f)

A mixture of **2d/2f** (200 mg, approx. 0.30 mmol), 4-methoxyphenylboronic acid (320 mg, 5.0 mmol) in toluene (12 mL) and ethanol (4 mL) at room temperature was stirred under argon, and K$_2$CO$_3$ (2 M, 20 mL) solution and Pd(PPh$_3$)$_4$ (70 mg, 0.06 mmol) were added. After the mixture was stirred for 30 min. at room temperature, the mixture was heated to 90 °C for 24 h with stirring. After cooling to room temperature, the mixture was quenched with water, extracted with CH$_2$Cl$_2$ (3 × 15 mL), washed with water and

brine. The organic extracts were dried with $MgSO_4$ and evaporated. The residue was firstly purified by column chromatography eluting with CH_2Cl_2-hexane (2:1) to give a mixture of 7-*tert*-butyl-1,3,5-tris-(4-methoxyphenyl)pyrene **3d** and 7-*tert*-butyl-1,3,5,9-tetrakis(4-methoxyphenyl)- pyrene **3f** (20 mg) as yellow prisms. The mixture was recrystallized from toluene solution to afford a few crystals of **3d**; the mixture was difficult to purify by HSCCC. Further detailed information (such ^{13}C NMR spectroscopy, MS, elemental analysis) of **3d** could not be obtained. Increasing the polarity of the eluant with CH_2Cl_2 gave only 7-*tert*-butyl-1,3,5,9-tetrakis(4-methoxyphenyl)pyrene **3f** (15 mg) as a yellow solid. The ^{1}H NMR spectrum of **3f** agreed with the reported values.[18] Mp: 407.5°C. IR (KBr): ν_{max} (cm^{-1}) = 2954, 1610, 1510, 1461, 1442, 1367, 1288, 1246, 1174, 1107, 1036, 831, 586, 543. ^{1}H NMR (300 MHz, $CDCl_3$): δ (TMS, ppm) 1.38 (s, 9H, *t*Bu), 3.90 (s, 6H, *OMe*), 3.92 (s, 6 H, *OMe*), 7.05(d, *J* = 1.6 Hz, 4H, Ar-*H*), 7.08 (d, *J* = 3.1 Hz, 4H, Ar-*H*), 7.57 (d, *J* = 8.8 Hz, 4H, Ar-*H*), 7.60 (d, *J* = 4.4 Hz, 4H, Ar-*H*), 7.92 (s, 1H,pyrene-*H*), 8.12 (s, 2H, pyrene-*H*), 8.30 (s, 2H, pyrene-*H*). ^{13}C NMR (75 MHz, $CDCl_3$): δ (TMS, ppm) 159.0, 158.9, 148.5, 139.1, 136.7,133.9, 133.7, 131.7, 131.2, 130.8, 129.7, 127.3, 125.6, 121.2, 113.9,113.8, 55.4, 31.7. FAB-HRMS: *m/z* calcd. for $C_{48}H_{42}O_4$ 682.84; found 682.19 [M$^+$]. Anal. Calcd for $C_{48}H_{42}O_4$: C, 84.43; H, 6.20;   found: C, 84.33; H, 6.52.

Synthesis of 7-*tert*-butyl-1,3,5,8-tetrakis(4-methoxyphenyl) pyrene (3e)

A mixture of 1,3,5,8-tetrabromo-7-*tert*-butylpyrene **2e** and 1,3,5,9-tetrabromo-7-*tert*-butylpyrene **2f** (200 mg, 0.35 mmol), 4-methoxyphenylboronic acid (303 mg, 2.0 mmol) in toluene (12 mL) and ethanol (4 mL) at room temperature was stirred under argon, and K_2CO_3 (2 M, 20 mL) solution and $Pd(PPh_3)_4$ (70 mg, 0.06 mmol)were added. After the mixture was stirred for 30 min. at room temperature, it was heated to 90 °C for 24 h with stirring. After cooling to room temperature, the mixture was quenched with water, extracted with CH_2Cl_2 (3 × 15 mL), washed with water and brine. The organic extracts were dried with $MgSO_4$ and evaporated. The residue was purified by column chromatography eluting with CH_2Cl_2 to give mixture of 7-*tert*-butyl-1,3,5,8-tetrakis(4-methoxy-phenyl)pyrene **3e** as a yellow powder. Mp: 240.0–241.2 °C. Recrystallization from (CH_2Cl_2/hexane, 4:1) gave **3e** in 42% yield (100 mg) as a yellow powder. Increasing the polarity of the eluant with CH_2Cl_2 afforded 7-*tert*-butyl-1,3,5,9-tetrakis(4-methoxy-phenyl)pyrene **3f** in 17% yield (40 mg) as a yellow solid.

7-*tert*-Butyl-1,3,5,8-tetrakis(4-methoxyphenyl)pyrene (3e) was obtained as pale yellow prisms (CH_2Cl_2-hexane, 3:1). Mp: 240.0−241.2 °C. IR (KBr): vmax (cm^{-1}) = 2954, 1607, 1507, 1462, 1440, 1288, 1246, 1177, 1105, 1037, 832, 808, 548, 526, 472. ^{1}H NMR (300 MHz, $CDCl_3$): δ (TMS, ppm) 1.30 (s, 9H, pyrene-*t*Bu), 3.88 (s, 3H, *OMe*), 3.89 (s, 3H, *OMe*),3.92 (s, 6H, *OMe*),7.00 (m,8H, Ar-*H*), 7.29 (d, *J* = 8.4 Hz, 2H, Ar-*H*), 7.35 (d, *J* = 9.5 Hz, 2H, pyrene-*H*), 7.54 (d, *J* = 8.61 Hz, 2H, 2H, Ar-*H*), 7.59 (d, *J* = 8.43 Hz, 2H, Ar-*H*), 7.60 (d, *J* = 8.61 Hz, 2H, Ar-*H*), 7.90 (s, 1H, pyrene-*H*),7.97 (d, *J* = 9.69 Hz, 1H, pyrene-*H*), 8.12 (s, 1H, pyrene-*H*), 8.51 (s, 1H, pyrene-*H*). ^{13}C NMR (100 MHz, $CDCl_3$): δ (TMS, ppm) 159.0, 158.9, 158.7, 146.0, 138.9, 136.9, 136.6, 136.3, 134.2, 133.6, 133.5, 133.1, 132.2, 131.62, 131.59, 131.2, 129.7, 129.5, 127.7, 127.0, 126.1, 125.5, 124.6, 124.5, 123.8, 122.5, 113.9, 113.81, 113.77, 113.71, 112.9, 55.35, 55.29, 37.5, 33.0. FAB-HRMS: *m/z* calcd. for $C_{48}H_{42}O_4$ 682.84; found 682.66 [M$^+$]. Anal. Calcd for $C_{48}H_{42}O_4$: C, 84.43; H, 6.20; found: C, 81.90; H, 6.15. The ^{1}H NMR spectrum of **3f** agreed with the reported values.[18]

7-*tert*-butyl-1,3,5,9-tetrakis(4-methoxyphenyl)pyrene (3f) was obtained as a yellow powder. Recrystallization from CH_2Cl_2-hexane (3:1) gave 7-*tert*-butyl-1,3,5,9-tetrakis(4-methoxyphenyl)pyrene (**3f**) in 65% yield (154 mg) as a yellow solid.

Crystallography for 3.

Diffraction data were collected using a Rigaku R-Axis Rapid for **3a**, or a Saturn724 for **3b**. A Bruker SMART CCD was used for **3c**, a SMART CCD for **3d**, and APEX II CCD diffractometers in the home laboratory for **3c** and **3f** or at the Advanced Light Source (ALS) Station 11.3.1 for **3e**.[39] Data were corrected for absorption on the basis of symmetry equivalent and repeated data and Lp effects. Structural solution and full matrix least-squares refinement were performed with the SHELXS-97 and SHELXL-97 or SHELXL-2013 software packages, respectively.[40] The structures were solved by direct methods and refined on *F*2 using all data.36 H atoms were constrained in a riding model. In **3c** the methyl groups on the *t*Bu group at C(17) was modeled with two sets of positions with major occupancy 63.4(12)%. Crystallographic Data (excluding structure factors) for the structures reported here have been deposited with the Cambridge Crystallographic Data Centre with deposition numbers, 965757 for **3a**, 879771 for **3b**, 965758 for **3c**, 965759 for **3d**, 965760 for **3e**, and 917257 for **3f**. Copies can be obtained free of charge upon application to CCDC, 12 Union Road, Cambridge CB2 1EZ, UK (Fax: +44 1223/336 033; e-mail: deposit@ccdc.cam.ac.uk).

Notes and references

[a] Beijing Institute of Graphic Communication, , Beijing 102600 P.R. China.

[b] Department of Applied Chemistry, Faculty of Science and Engineering, Saga University, Honjo-machi 1, Saga 840-8502 Japan.E-mail: yamatot@cc.saga-u.ac.jp.

[c] Emergent Molecular Function Research Group, RIKEN Center for Emergent Matter Science (CEMS), Wako, Saitama 351-0198, Japan.

d Key Laboratory of Macrocyclic and Supramolecular Chemistry of Guizhou Province, Guizhou University, Guiyang, Guizhou, 550025, P. R. China.

e Department of Chemistry, The University of Hull, Cottingham Road, Hull, Yorkshire, HU6 7RX, UK..

f Chemistry Department, Loughborough University, Loughborough, LE113TU, UK..

g ALS, Berkeley Lab, 1 Cyclotron Road, MS2-400, Berkeley, CA 94720,USA.

1   (*a*) T. M. Figueira-Duarte and K. Müllen, *Chem. Rev.*, 2011, **111**, 7260–7314; (*b*) J-Y. Hu and T. Yamato, *Organic Light Emitting Diode - Material, Process and Devices*, 2011, 21–60; (*c*) P. C. Bevilacqua, R. Kierzek and K. A. Johnson, *Science*, 1992, **258**, 1355–1358.

2   A. G. Crawford, A. D. Dwyer, Z-Q. Liu, A. Steffen, A. Beeby, L.-O. Pålsson, D. L. Tozer and T. B. Marder, *J. Am. Chem. Soc.*, 2011, **133,** 13349–13362.

3   D. N. Coventry, A. S. Batsanov, A. E. Goeta, J. A. K. Howard, T. B. Marder and R. N. Perutz, *Chem. Commun.,* 2005, 2172–2174.

4   A. G. Crawford, Z.-Q. Liu, I. A. I. Mkhalid, M-H. Thibault, N. Schwarz, G. Alcaraz, A. Steffen, J. C. Collings, A. S. Batsanov, J. A. K. Howard and T. B. Marder, *Chem. Eur. J.,* 2012, **18**, 5022–5035.

5   S.-T. Lin, Y.-F. Jih and P. P. Fu, *J. Org. Chem.,*1996, **61,** 5271–5273.

6   H. Vollmann, M. Becker, M. Correl and H. Streeck, *Justus Liebigs Ann. Chem.*, 1937, **531**, 1–159

7   T. Yamato, A. Miyazawa and M. Tashiro, *J. Chem. Soc. Perkin Trans. 1,* 1993, 3127–3137.

8   T. Yamato, M. Fujimoto, A. Miyazawa and K. Matsuo, *J. Chem. Soc. Perkin Trans. 1*, 1997, 1201–1207.

9   J. Hu, D. Zhang and F. W. Harris, *J. Org. Chem.*, 2005, **70**, 707–708.

10   (*a*) X. Feng, F. Iwanaga, J.-Y. Hu, H. Tomiyasu, M. Nakano, C. Redshaw, M. R. J. Elsegood and T. Yamato, *Org. Lett.*, 2013, **15**, 3594–3597; (*b*) B.-X. Gao, M. Wang, Y.-X. Cheng, L.-X. Wang, X.-B. Jing and F.-S. Wang, *J. Am. Chem. Soc.,* 2008, **130**, 8297–8306; (*c*) N. Kulisic, S. Moreab and A. Mateo-Alonso, *Chem. Commun.*, 2011, **47**, 514–516. (d) A. Mateo-Alonso, *Chem. Soc. Rev.,* 2014, DOI: 10.1039/c4cs00119b.

11   J. Se. Kim and D. T. Quang, *Chem. Rev.*, 2007, **107**, 3780–3799.

12   L. Chouai, F.-Y. Wu, Y. Jang and R. P. Thummel, *Eur. J. Inorg. Chem.,* 2003, 2774–2782.

13   G. Venkataramana and S. Sankararaman, *Org. Lett.,* 2006, **8**, 2739–2742.

14   J. N. Moorthy, P. Natarajan, P. Venkatakrishnan, D.-F. Huang and T. Chow, *Org. Lett.,* 2007, **9**, 5215–5218.

15   Y. Niko, S. Kawauchi, S. Otsu, K. Tokumaru and G.-I. Konishi, *J. Org. Chem.*, 2013, **78**, 3196–3207.

16   X-L. Ni, X. Zeng, C. Redshaw and T. Yamato, *J. Org. Chem.*, 2011, **76**, 5696–5702.

17   (*a*) J.-Y. Hu, X-L. Ni, X. Feng, M. Era, M. R. J. Elsegood, S. J. Teatd and T. Yamato, *Org. Biomol. Chem.* 2012, **10**, 2255–2262; (*b*) J.-Y. Hu, M. Era, M. R. J. Elsegood and T. Yamato, *Eur. J. Org. Chem.,* 2010, 72–79.

18   X. Feng, J.-Y. Hu, F. Iwanaga, N. Seto, C. Redshaw, M. R. J. Elsegood and T. Yamato, *Org. Lett.*, 2013, **15,** 1318–1321.

19   (*a*) L. Zöphel, D. Beckmann, V. Enkelmann, D. Chercka, R. Rieger and K. Müllen, *Chem. Commun.*, 2011, **47**, 6960–6962; (*b*) L. Zöphel, V. Enkelmann and K. Müllen, *Org. Lett.*, 2013, **15**, 804–807.

20   S. Kawano, M. Baumgarten, D. Chercka, V. Engkelmannand K. Müllen, *Chem. Commun.,* 2013, **49,** 5058–5060.

21   (a) J.-Y. Hu, Y.-J. Pu, G. Nakata, S. Kawata, H. Sasabeand J. Kido, *Chem. Commun.*, 2012, **48**, 8434–8436; (b) Y.-L. Qiao, J. Zhang, W. Xua, D.-B. Zhu, *Tetrahedron*, 2011, **67**, 3395–3405.

22   (*a*) X. Feng, J-Y. Hu, L. Yi, N. Seto, Z. Tao, C. Redshaw, M. R. J. Elsegood and T. Yamato, *Chem. Asian J.*, 2012, **7**, 2854–2863; (*b*) T. M. Figueira-Duarte, S. C. Simon, M. Wagner, S. I. Druzhinin, K. A. Zachariasse and K. Müllen, *Angew. Chem. Int. Ed.,* 2008, **47**, 10175–10178.

23   L. M. Sayre and F. R. Jensen, *J. Am. Chem. Soc.*, 1979, **101**, 6001–6008.

24   (*a*) A. Burritt, J. M. Coxon and P. J. Steel, *J. Org. Chem.,* 1996, **61**, 4328–4335; (*b*) X. Gao, W. Qiu, X. Yang, Y. Liu, Y. Wang, H. Zhang, T. Qi, Y. Liu, K. Lu, C. Du, Z. Shuai, G. Yu and D.-B. Zhu, *Org. Lett.*, 2007, **9**, 3917–3920.

25   J. Inoue, K. Fukui, T. Kubo, S, Nakazawa, K. Sato, D. Shiomi, Y. Morita, K. Yamamoto, T. Takui and K. Nakasuji, *J. Am. Chem. Soc.*, 2001, **123**, 12702–12703.

26   W. E. Moffitt and C. A. Coulson, *Proc. Phys. Soc.*, *1948*, **60**, 309–315.

27   A. S. Batsanov, J. A. K. Howard, D. Albesa-Jové, J. C. Collings, Z.Q. Liu, I. A. I. Mkhalid, M.-H. Thibault and T. B. Marder, *Cryst. Growth Des.*, 2012, **12**, 2794–2802.

28   V. de Halleux, J.-P. Callbert, P. Brocorens, J. Cornil, J.-P. Declercq, J.-L. Brédasand Y. Geerts, *Adv. Funct. Mater.*, 2004, **14**, 649–659.

29   K. R. J. Thomas, J. T. Lin, Y.-T. Tao, C.-H. Chuen, *Chem. Mater.*, 2002, **14**, 2796–2802.

30   (*a*) F. Polo, F. Rizzo, M. Veiga-Gutierrez, L. D. Cola and S. Quici, *J. Am. Chem. Soc.*, 2012, **134**, 15402−15409; (*b*) S. Kato, S. Shimizu, H. Taguchi, A. Kobayashi, S. Tobita and Y. Nakamura, *J. Org. Chem.*, 2012, **77**, 3222−3232.

31   P. Tyagi, A. Venkateswararao and K. R. J. Thomas, *J. Org. Chem.*, 2011, **76**, 4571–4581.

32   Y. Li, J. Ding, M. Day, Y. Tao, J. Lu and M. D'iorio, *Chem. Mater.*, 2004, **16**, 2165–2173.

33   C.-G. Wang, S.-Y. Chen, K. Wang, S.-S. Zhao, J.-Y. Zhang and Y. Wang, *J. Phys. Chem. C.*, 2012, **116**, 17796−17806.

34   Z.-Q. Liu, Y.-Y. Wang, Y. Chen, J. Liu, Q. Fang, C. Kleeberg and T. B. Marder, *J. Org. Chem.*, 2012, **77**, 7124−7128.

35   Y. Miura, E. Yamano, A. Tanaka and J. Yamauchi, *J. Org. Chem.*, 1994, **59**, 3294–3300.

36   M. J. Frisch, G. W. Trucks, H. B. Schlegel, G. E. Scuseria, M. A. Robb, J. R. Cheeseman, J. A., Jr. Montgomery, T. Vreven, K. N. Kudin, J. C. Burant, J. M. Millam, S. S. Iyengar, J. Tomasi, V. Barone, B. Mennucci, M. Cossi, G. Scalmani, N. Rega, G. A. Petersson, H. Nakatsuji, M. Hada, M. Ehara, K. Toyota, R. Fukuda, J. Hasegawa, M. Ishida, T. Nakajima, Y. Honda, O. Kitao, H. Nakai, M. Klene, X. Li, J. E. Knox, H. P. Hratchian, J. B. Cross, V. Bakken, C. Adamo, J. Jaramillo, R. Gomperts, R. E. Stratmann, O. Yazyev, A. J. Austin, R. Cammi, C. Pomelli, J. W. Ochterski, P. Y. Ayala, K. Morokuma, G. A. Voth, P. Salvador, J. J. Dannenberg, V. G. Zakrzewski, S. Dapprich, A. D. Daniels, M. C. Strain, O. Farkas, D. K. Malick, A. D. Rabuck, K. Raghavachari, J. B. Foresman, J. V. Ortiz, Cui, Q.; Baboul, A. G.; Clifford, S.; Cioslowski, J.; Stefanov, B. B.; G. Liu, A. Liashenko, P. Piskorz, I. Komaromi, R. L. Martin, D. J.

Fox, T. Keith, M. A. Al-Laham, C. Y. Peng, A. Nanayakkara, M. Challacombe, P. M. W. Gill, B. Johnson, W. Chen, M. W. Wong, C. Gonzalez, J. A. Pople, *Gaussian 03*, revision C.02, Gaussian, Inc., Wallingford CT, **2004**.

Iron (III) bromide catalyzed bromination of 2-*tert*-butylpyrene and corresponding positions-dependent aryl-functionalized pyrene derivatives

Xing Feng, Jian-Yong Hu, Hirotsugu Tomiyasu, Zhu Tao, Carl Redshaw, Mark R. J. Elsegood, Lynne Horsburgh, Simon J. Teat, Xian-Fu Wei and Takehiko Yamato
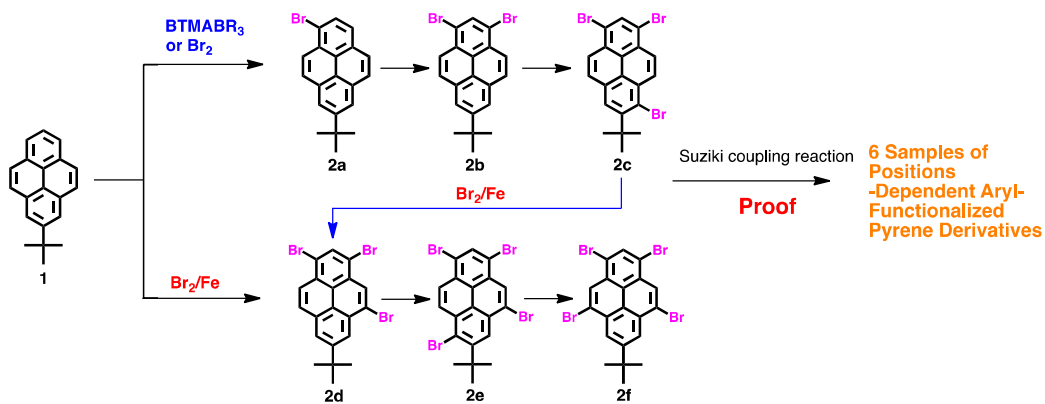
The present work probes the bromination mechanism of 2-*tert*-butylpyrene

Supporting Information for

Iron (III) Bromide Catalyzed Bromination of 2-*tert*-Butylpyrene and Corresponding Positions-Dependent Aryl-Functionalized Pyrene Derivatives

Xing Feng,[a,b] Jian-Yong Hu,[b,c] Hirotsugu Tomiyasu,[b] Zhu Tao,[d] Carl Redshaw,[e] Mark R.J. Elsegood,[f] Lynne Horsburgh,[f] Simon J. Teat,[g] Xian-Fu Wei,[a] and Takehiko Yamato[*b]

[a] *School of Printing and Packing Engineering, Beijing Institute of Graphic Communication, 1 Xinghua Avenue (Band Two), Daxing, Beijing 102600 P.R. China,*

[b] *Department of Applied Chemistry, Faculty of Science and Engineering, Saga University, Honjo-machi 1, Saga 840-8502 Japan. E-mail: yamatot@cc.saga-u.ac.jp*

[c] *Emergent Molecular Function Research Group, RIKEN Center for Emergent Matter Science (CEMS), Wako, Saitama 351-0198, Japan*

[d] *Key Laboratory of Macrocyclic and Supramolecular Chemistry of Guizhou Province, Guizhou University, Guiyang, Guizhou, 550025, P. R. China.*

[e] *Department of Chemistry, The University of Hull, Cottingham Road, Hull, Yorkshire, HU6 7RX, UK.*

[f] *Chemistry Department, Loughborough University, Loughborough, LE113TU, UK.*

[g] *ALS, Berkeley Lab, 1 Cyclotron Road, MS2-400, Berkeley, CA 94720,USA.*

Table of Contents

1 300 MHz ^{1}HNMR sprectrum of **1** and **2a**

2 300 MHz ^{1}HNMR sprectrum of **2b** and **2c**

3 300 MHz ^{1}HNMR sprectrum of **2d** and **2e**

4 300 MHz ^{1}HNMR sprectrum of **2f** and **3a**

5 300 MHz ^{1}HNMR sprectrum of **3b** and **3c**

6 300 MHz ^{1}HNMR sprectrum of **3b** and 400 MHz ^{1}HNMR

sprectrum **3c**

7 300 MHz ^{1}HNMR sprectrum of **3e** and **3f**

8 100 MHz ^{13}CNMR sprectrum of **3a** and **3b**

9 100 MHz ^{13}CNMR sprectrum of **3c** and **3e**

10 75 MHz ^{13}CNMR sprectrum of **3f**

11 the key crystallographic data of **3**

12 Mechanism of bromination of 2-*tert*-butyl pyrene
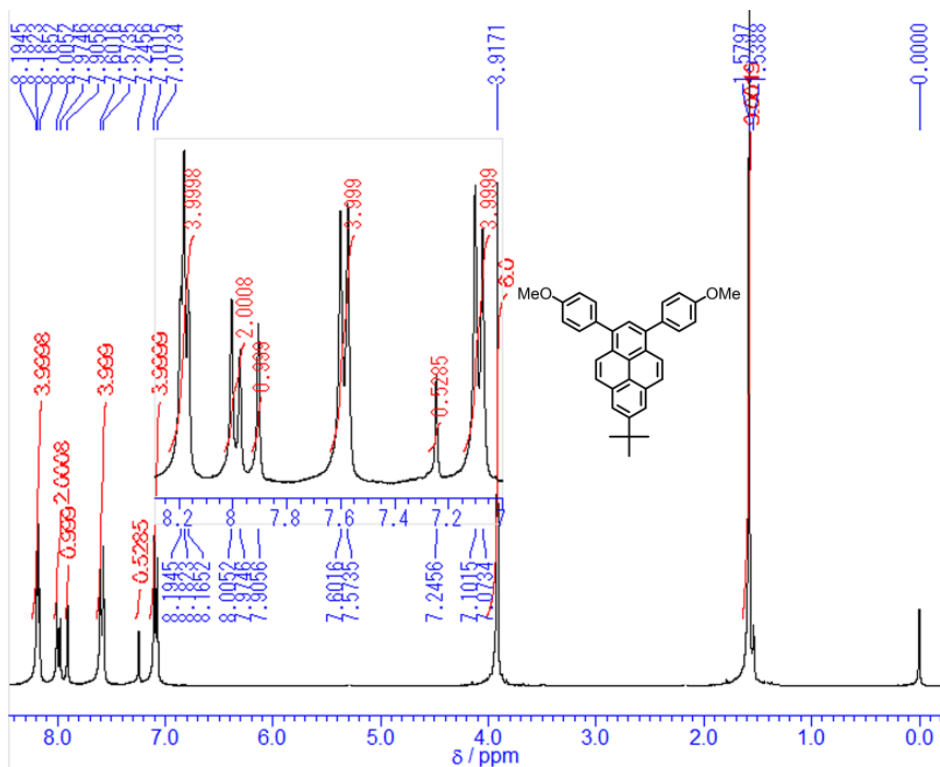
13 Quantum Chemistry Computation

Copy of NMR Spectra
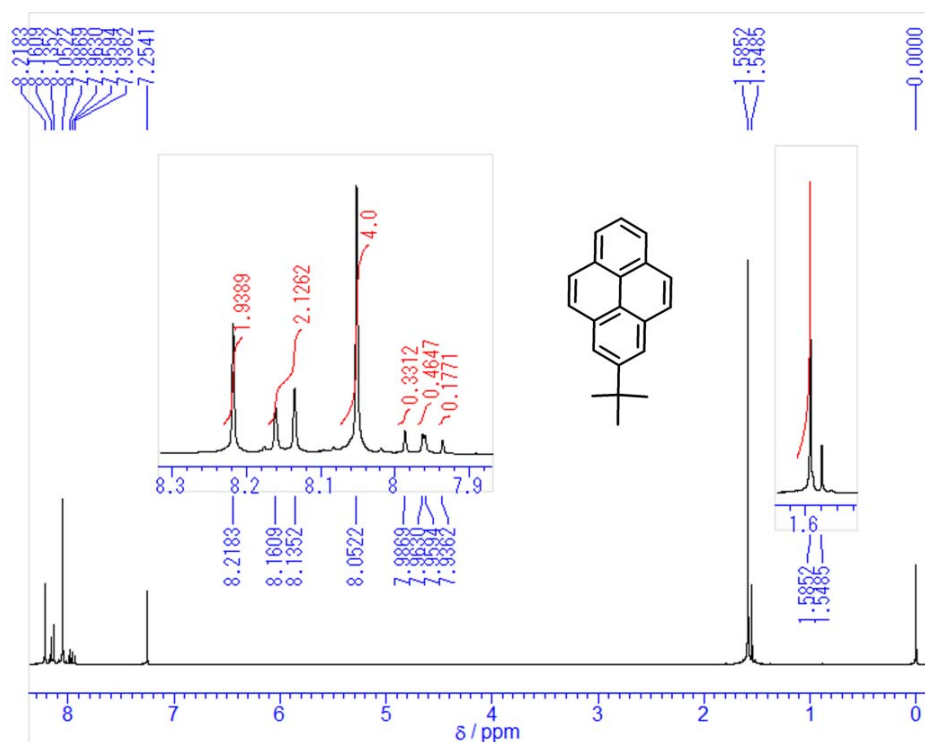
Figure S1-1 ^{1}H-NMR spectrum (300 MHz, 293K, * CDCl$_3$) for **1** including an expansion of the aromatic region.
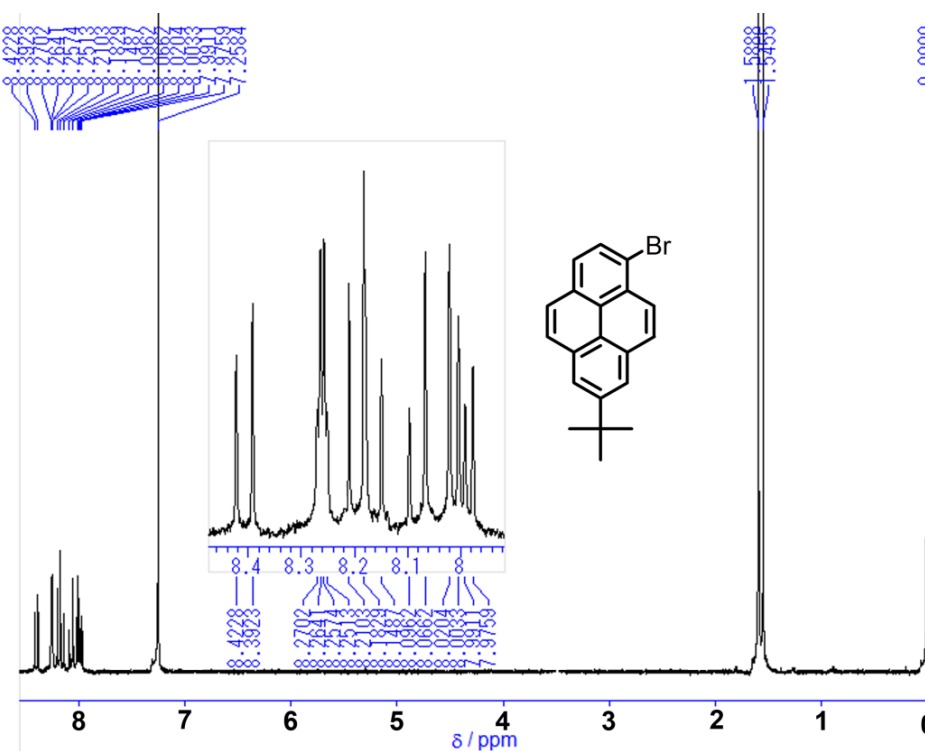
Figure S1-2 ^{1}H-NMR spectrum (300 MHz, 293K, * CDCl$_3$) for **2a** including an expansion of the aromatic region.
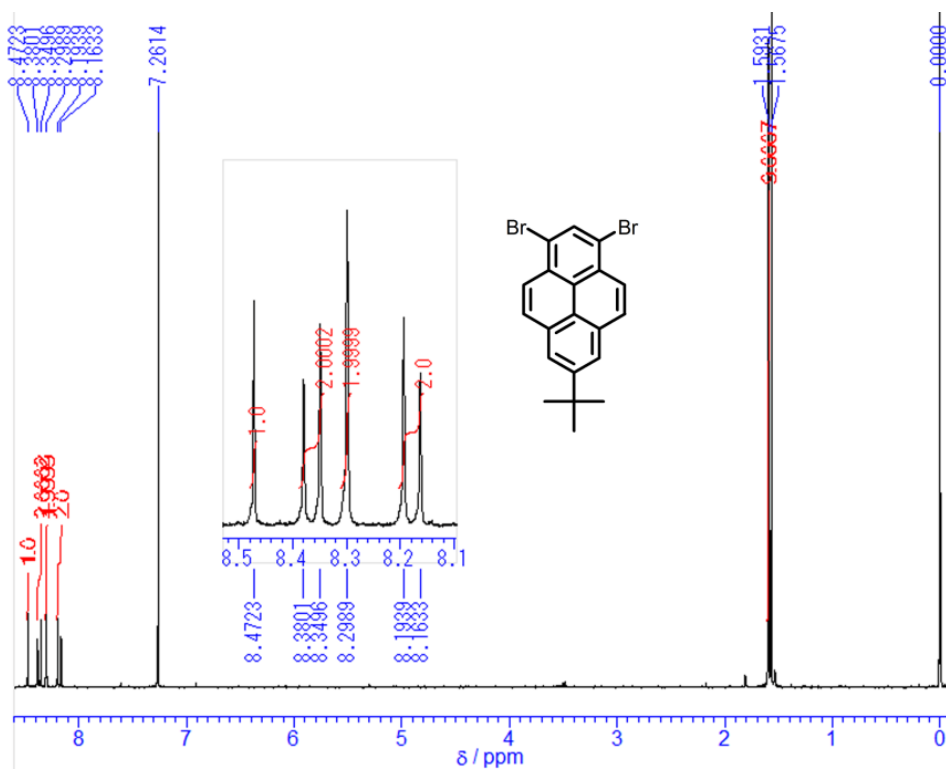
Figure S1-3 ^{1}H-NMR spectrum (300 MHz, 293K, * CDCl₃) for **2b** including an expansion of the aromatic region.
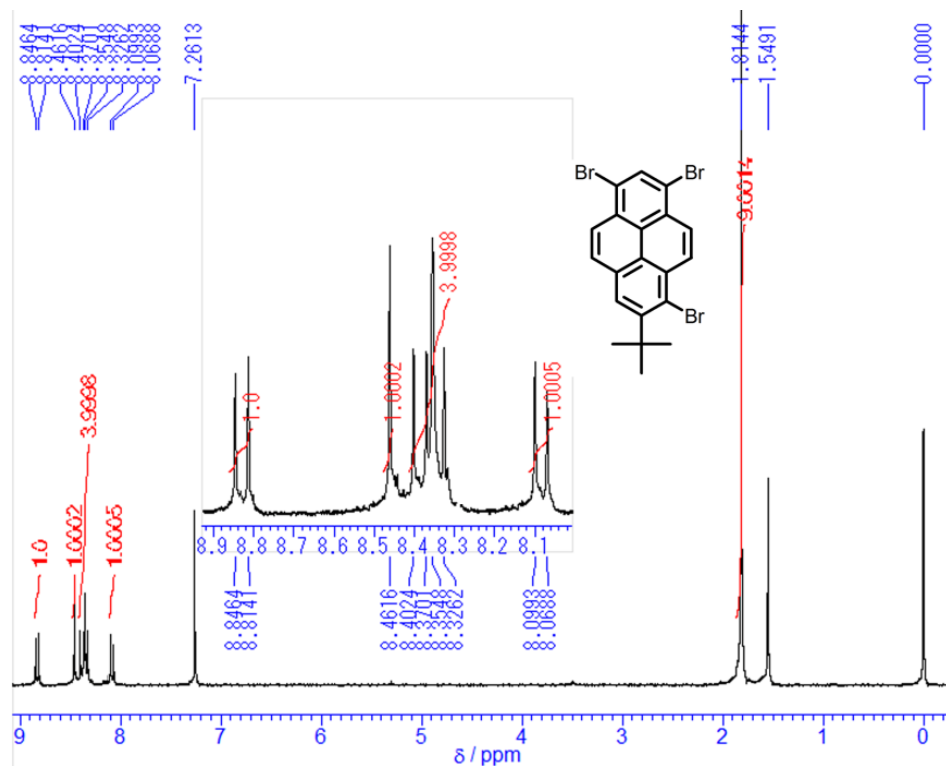
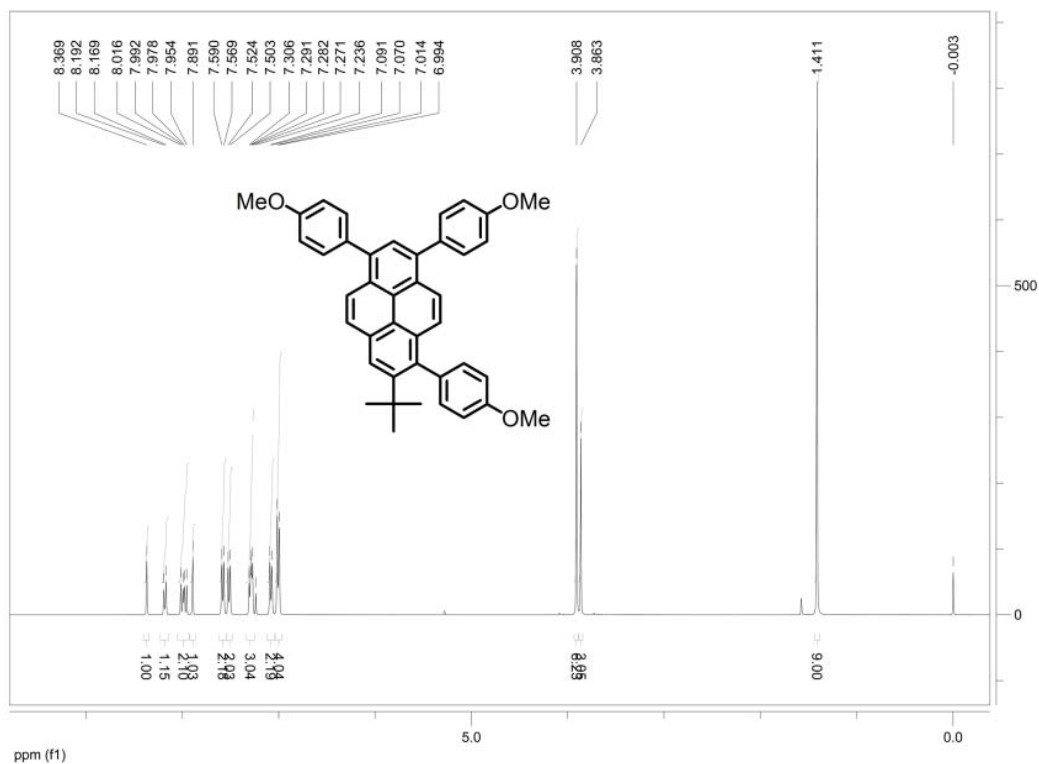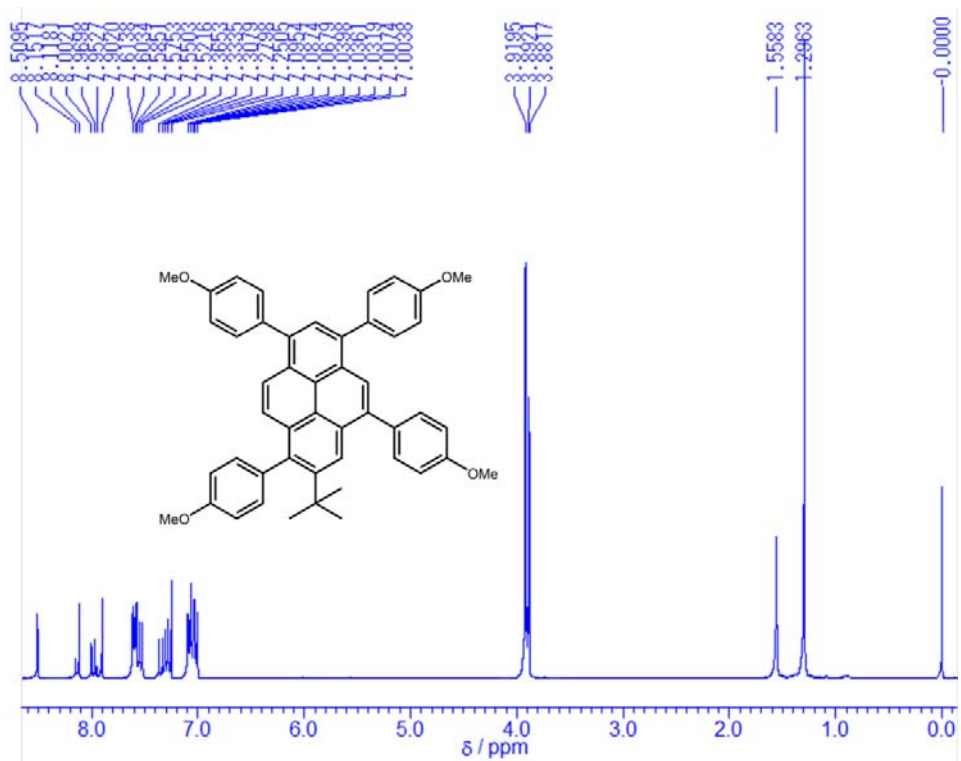**Figure S1-4** ^{1}H-NMR spectrum (300 MHz, 293K, * CDCl₃) for **2c** including an expansion of the aromatic region.
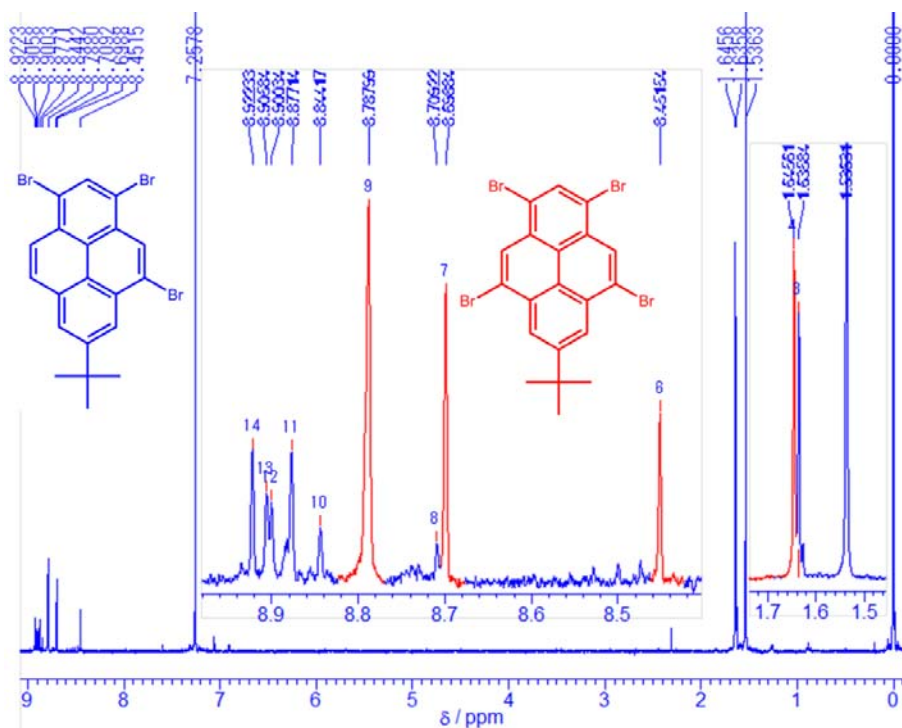
Figure S1-5 ^{1}H-NMR spectrum (300 MHz, 293K, * CDCl$_3$) of mixture **2d** and **2f** including an expansion of the aromatic region.
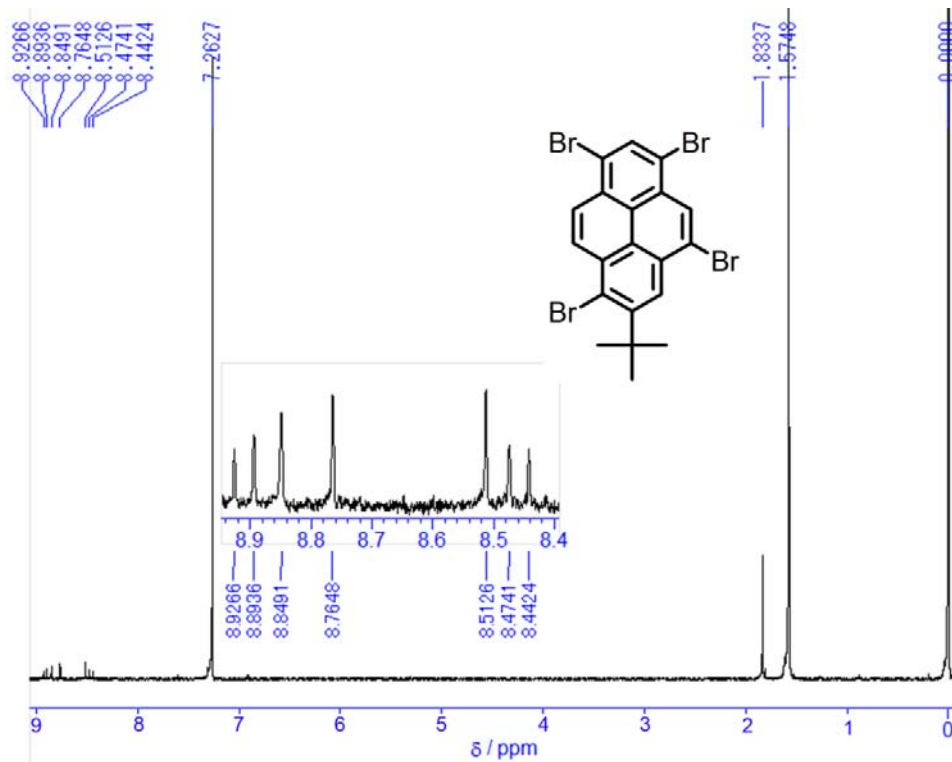
Figure S1-6 ^{1}H-NMR spectrum (300 MHz, 293K, * CDCl$_3$) for **2e** including an expansion of the aromatic region.
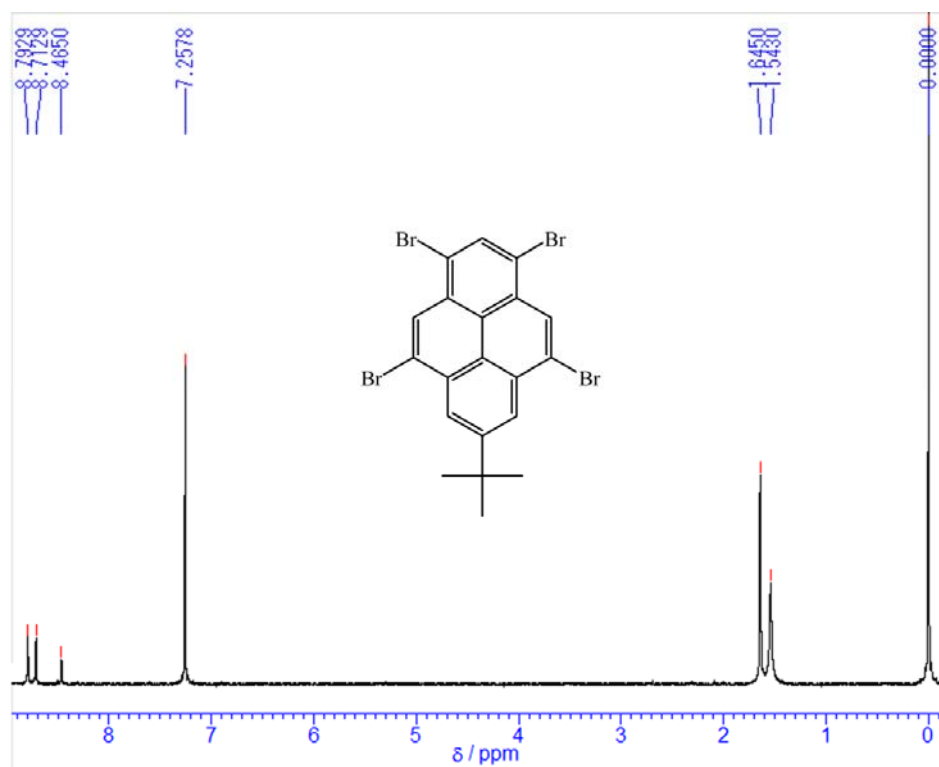
Figure S1-14 ^{1}H-NMR spectrum (300 MHz, 293K, * CDCl$_3$) for **3f**.
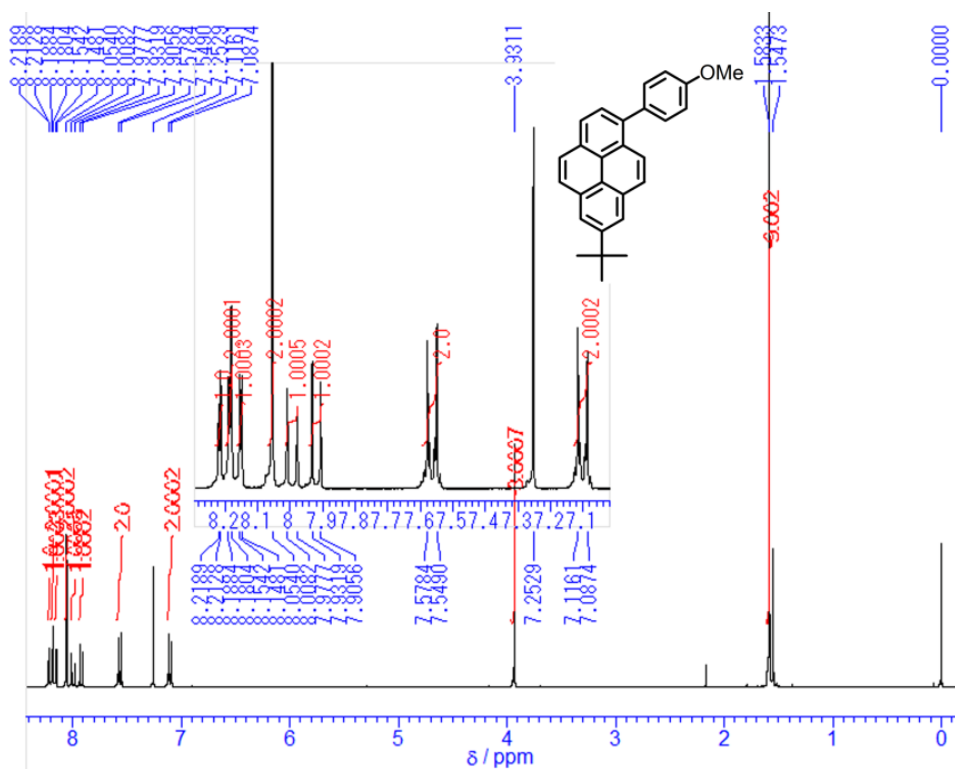
Figure S1-8 ^{1}H-NMR spectrum (300 MHz, 293K, * CDCl$_3$) for **3a** including an expansion of the aromatic region.

Figure S1-9 ^{1}H-NMR spectrum (300 MHz, 293K, * CDCl₃) for **3b** including an expansion of the aromatic region.

Figure S1-10 ^{1}H-NMR spectrum (400 MHz, 293K, * CDCl₃) for **3c**.

Figure S1-11 ^{1}H-NMR spectrum (300 MHz, 293K, * CDCl$_3$) for **3e**.
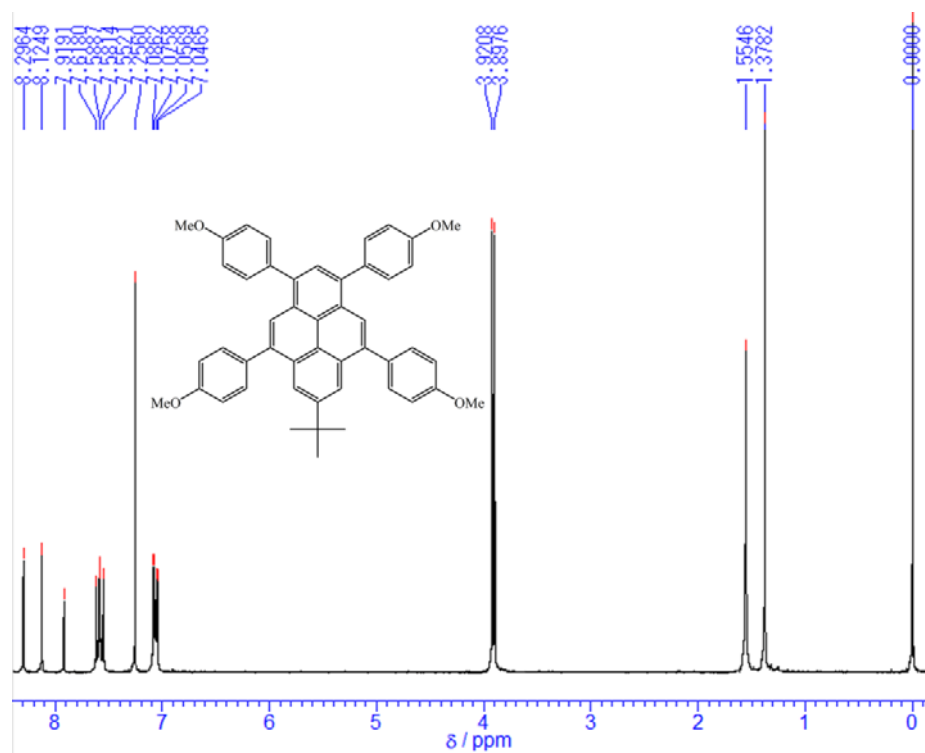
Figure S1-12 ^{1}H-NMR spectrum (300 MHz, 293K, * CDCl$_3$) for **3f**.
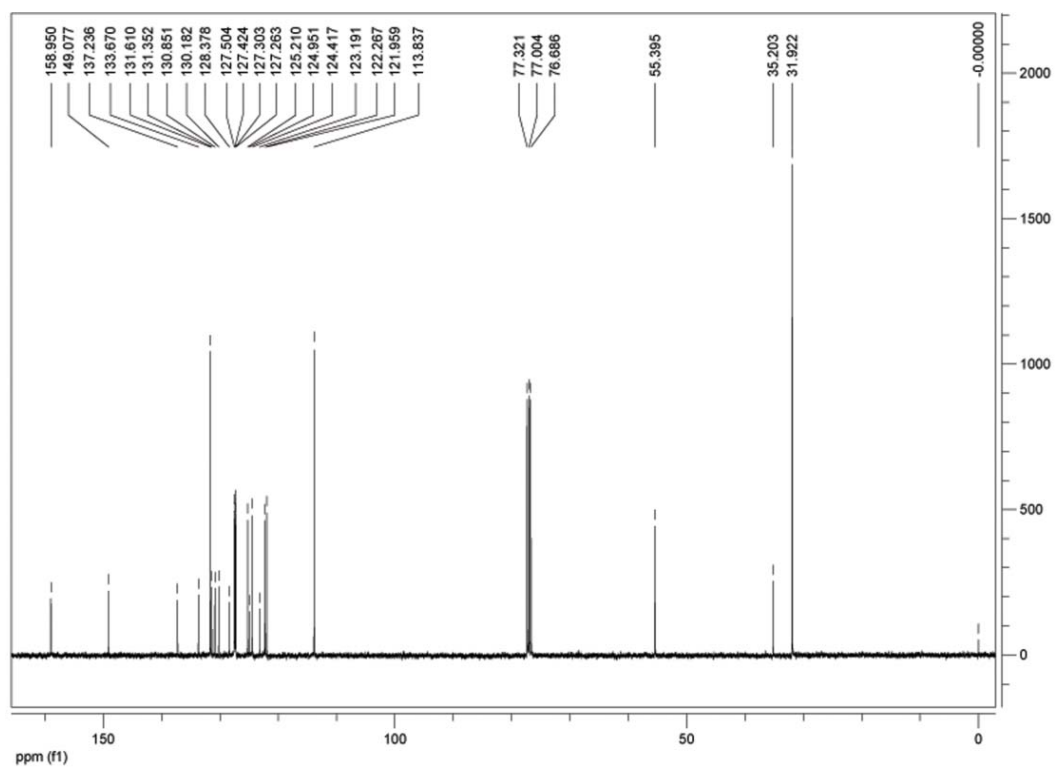
Figure S1-13 ^{13}C-NMR spectrum (100 MHz, 293K, * CDCl$_3$) for **3a**.
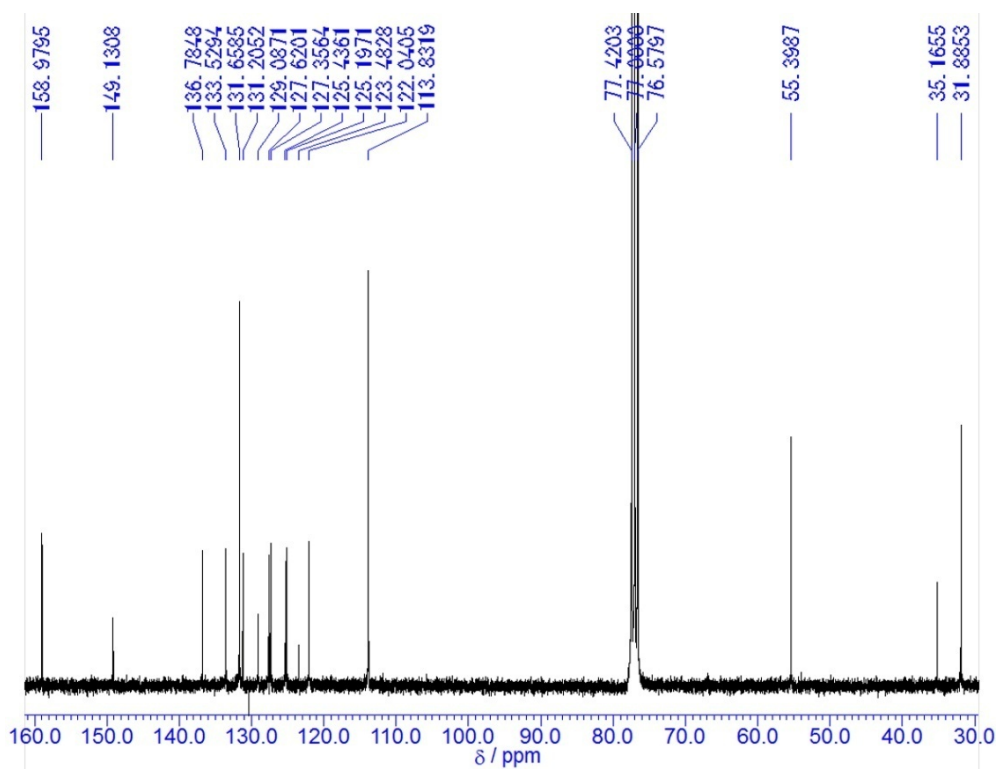
Figure S1-14 ^{13}C-NMR spectrum (75 MHz, 293K, * CDCl$_3$) for **3b**.
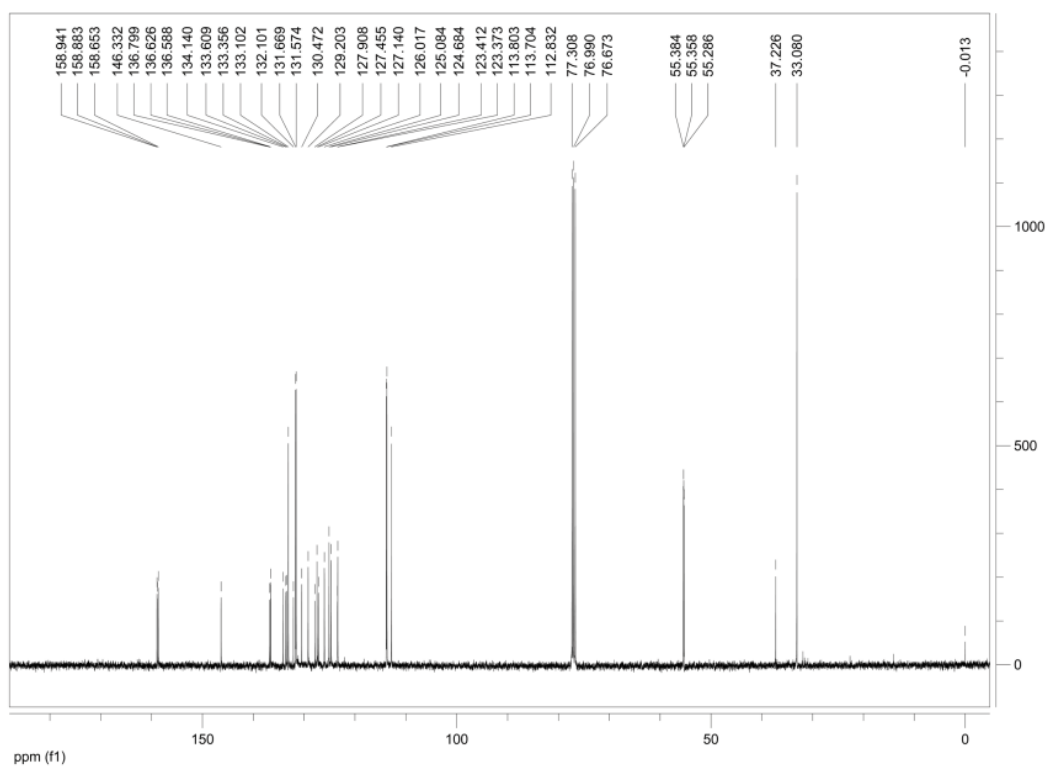
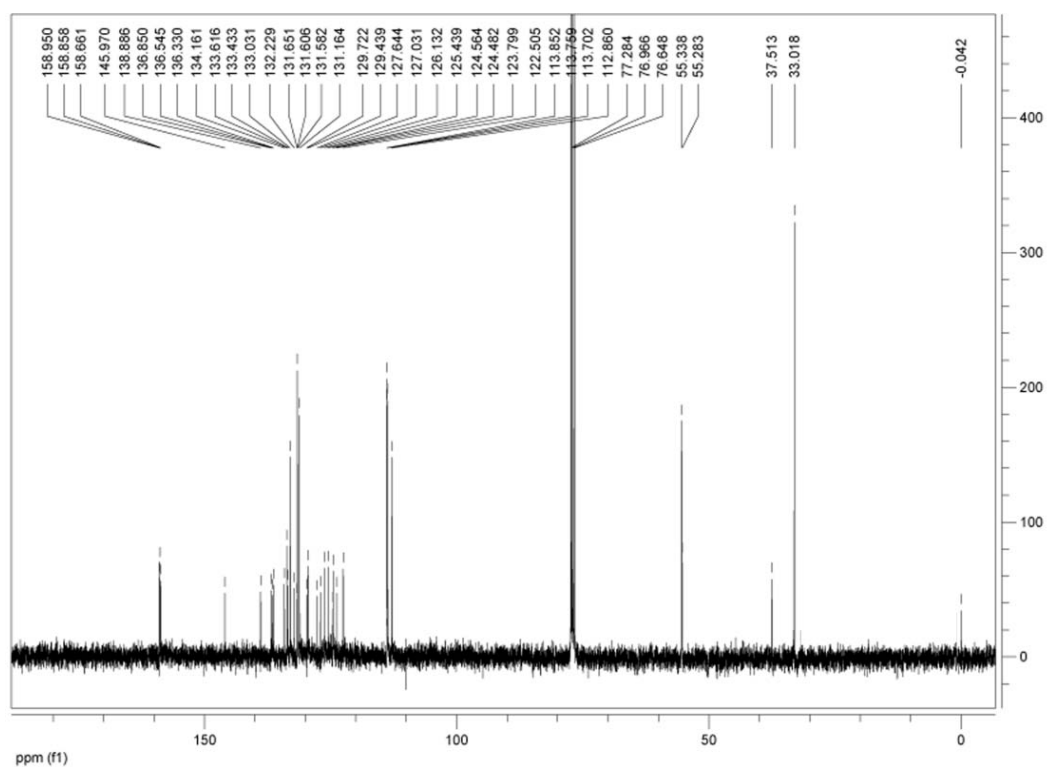**Figure S1-15** ^{13}C-NMR spectrum (100 MHz, 293K, * CDCl$_3$) for **3c**.

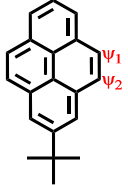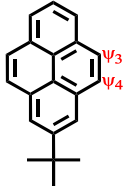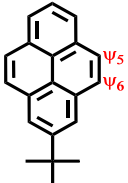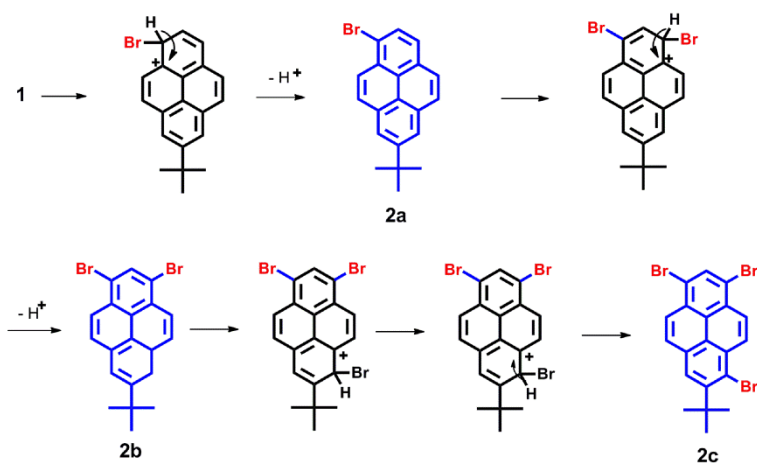**Figure S1-16** ^{13}C-NMR spectrum (100 MHz, 293K, * CDCl$_3$) for **3e**.
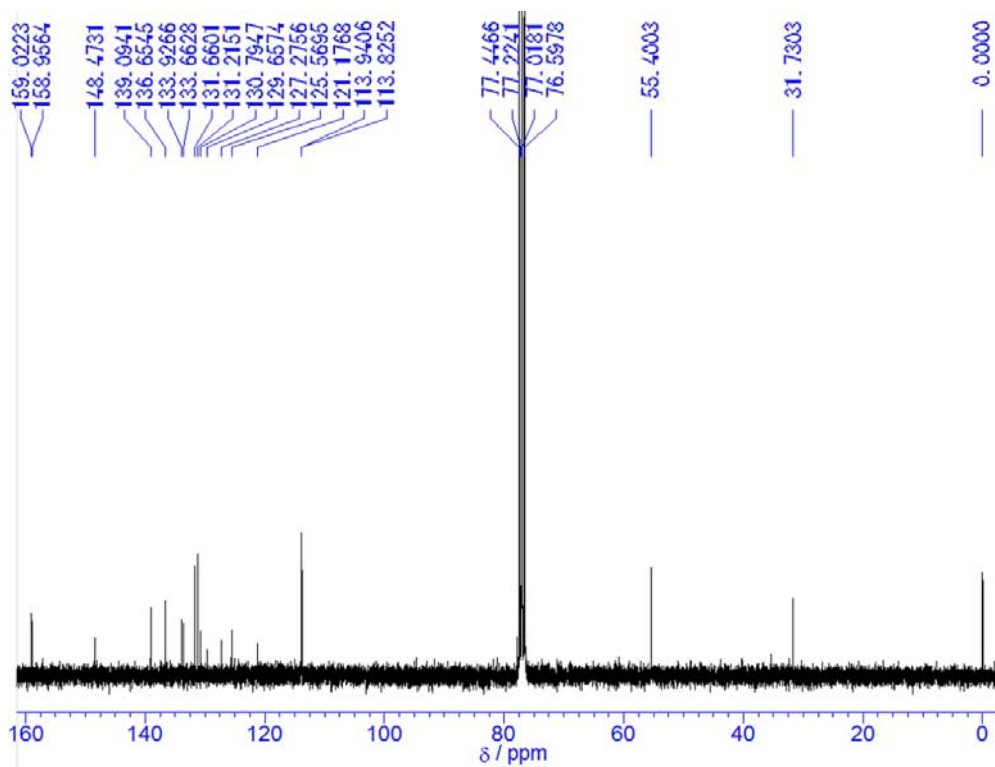
Figure S1-17 ^{13}C-NMR spectrum (75 MHz, 293K, * CDCl$_3$) for **3f**.

Mechanism of bromination of 2-*tert*-butyl pyrene

Table S1 the ratio of benzenoid rings and double bonds[1]

Structure	Ratio	Coefficients	Nb	Ne
	$\psi1$: $\psi2$	1.31	2	2
	$\psi3$: $\psi4$	1.27	3	2
	$\psi5$: $\psi6$	1.00	1	1

Nb=number of benzenoid rings ;Ne=number of exposed bonds

Scheme S1 Possible regioselective bromination mechanism of **1**

[1] Moffitt, W. E.; Coulson, C. A. *Proc. Phys. Soc.*; **1948**, *60*, 309–315.

X-Ray diffraction data

Table S2 Summary of crystal data of pyrene derivatives **3**

Parameter	3a	3b	3c	3d	3e	3f
Empirical formula	$C_{27}H_{24}O$	$C_{34}H_{30}O_2$	$C_{41}H_{36}O_3$	$C_{41}H_{36}O_3$	$C_{48}H_{42}O_4$	$C_{48}H_{42}O_4$
Formula weight [g mol^{-1}]	364.49	470.61	576.70	576.70	682.81	682.82
Crystal system	orthorhombic	monoclinic	Monoclinic	triclinic	monoclinic	triclinic
Space group	$P\,b\,c\,a$	$P2_1/c$	$P2_1/c$	$P\,\text{-}1$	$P2_1/c$	$P\text{-}1$
a [Å]	34.643(4)	18.815(14)	9.136 (2)	10.299(6)	17.5703(6)	12.642(2)
b [Å]	11.0927(16)	15.629(11)	17.638 (4)	12.845(7)	8.8286(3)	12.960(2)
c [Å]	10.1811(13)	8.851(6)	19.524 (4)	13.482(12)	24.0368(9)	13.854(2)
α [°]	-	-		111.174(9)		86.048(2)°
β [°]	-	103.255(9)	98.252 (4)°	103.142(10)	101.190(2)	67.354(2)°
γ [°]	-	-		102.291(7)		60.942(2)°
Volume [Å^3]	3912.4(9)	2533(3)	3113.5 (12)	1531.8(19)	3657.7(2)	1811.4(5)
Z	8	4	4	2	4	2
Density, calcd [gm^{-3}]	1.237	1.234	1.230	1.250	1.240	1.252
Temperature [K]	113	123	150	296(2)	100(2)	150(2)
Unique reflns	3495	5722	7734	5187	73709	10122
Obsdreflns	2925	4734	6709	3075	13376	7260
Parameters	257	330	500	397	637	476
R_{int}	0.0475	0.0640	0.034	0.0535	0.0404	0.0255
R[I>2σ(I)]^a	0.0360	0.1034	0.048	0.0911	0.0441	0.0475
wR[I>2σ(I)]^b	0.1041	0.3036	0.146	0.2649	0.1317	0.1413
GOF on F^2	1.123	1.186	1.06	0.988	1.035	1.047

[a] Conventional R on F_{hkl}: $\Sigma||F_o| - |F_c||/\sigma|F_o|$. [b] Weighted R on $|F_{hkl}|^2$: $\Sigma[w(F_o^2 - F_c^2)2]/\Sigma[w(F_o^2)^2]^{1/2}$

Quantum Chemistry Computation

1

2a   **2b**   **2c**

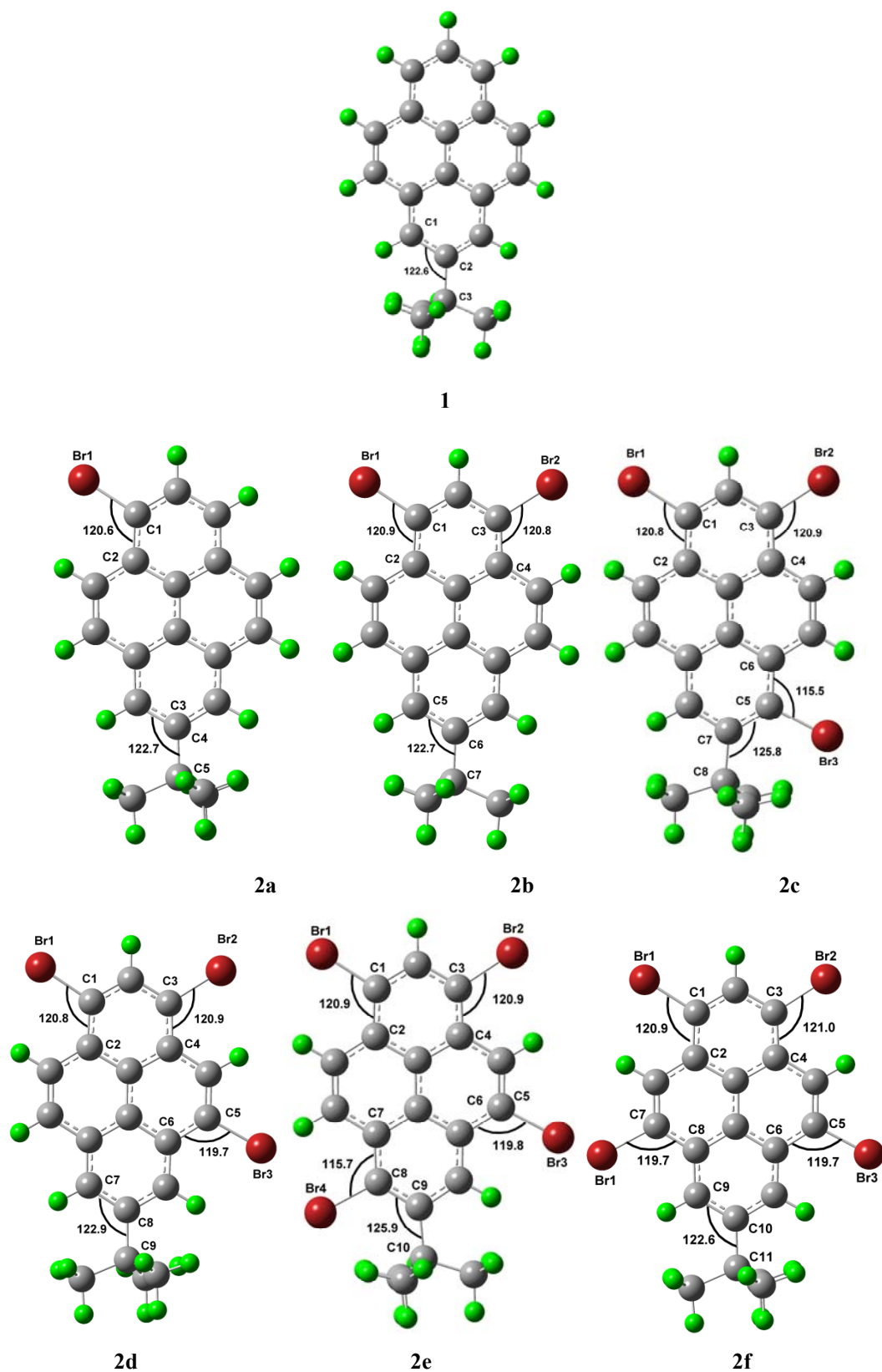**2d**   **2e**   **2f**

Figure S2-2 Geometric structures of bromo-substituted pyrene **2** in the FeBr$_3$-catalyzed reactions. The unit of angle is in $^{\circ}$.
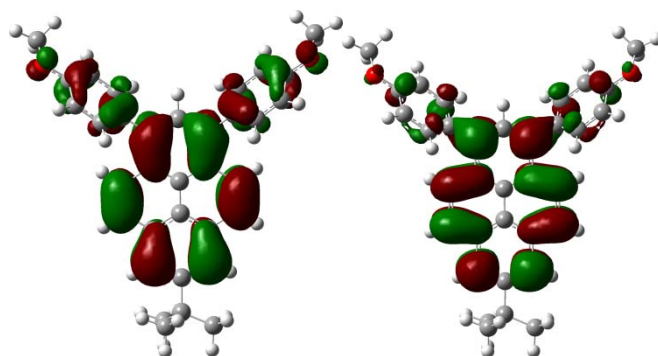
Figure S3-1 Computed molecular orbital plots (B3LYP/6–31G*) for **3b**: The left plots represent the HOMOs, and the right plots represent the LUMOs.
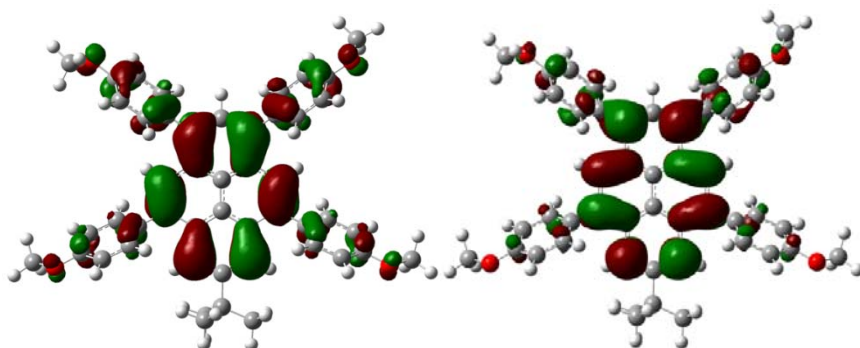

Figure S3-2 Computed molecular orbital plots (B3LYP/6–31G*) for **3f**: The left plots represent the HOMOs, and the right plots represent the LUMOs.
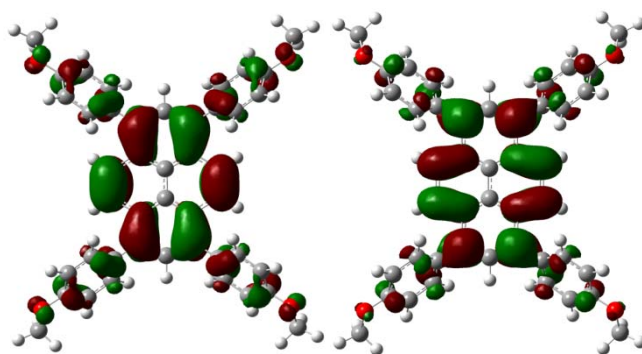

Figure S3-3 Computed molecular orbital plots (B3LYP/6–31G*) for **4**: The left plots represent the HOMOs, and the right plots represent the LUMOs.

Table S**3**. Physical and electrochemical properties of compounds **3**, **4** and **5**.

Compound	LUMO (eV)[a]	LUMO (eV)[b]	$E_{ox}^{1/2[c]}$ (eV)	$E_{ox}^{onset[d]}$ (eV)	$E_{ox (Fc)}^{onset[d]}$ (eV)	HOMO (eV)	HOMO-LUMO ΔE (eV)
3a	-1.41	nd	nd	nd	nd	-5.06[a] / nd	3.65[a] / 3.30 [e]
3b	-1.41	-2.27	1.45	1.36	0.66	-4.93 / -5.44[b]	3.51 / 3.17
3c	-1.39	-2.13	1.51	1.32	0.64	-4.84 / -5.06	3.45 / 3.13
3d	-1.39	nd	nd	nd	nd	-4.82 / nd	3.43 / nd
3e	-1.39	-2.33	1.64	1.59	0.65	-4.76 / -5.36	3.37 / 3.03
3f	-1.36	-2.34	1.67	1.61	0.65	-4.76 / -5.37	3.40 / 3.03
4	-1.47	nd	nd	nd	nd	-4.71 / nd	3.24 / 2.94
5	-1.22	nd	nd	nd	nd	-4.93 / nd	3.70 / 3,31

[a] DFT/B3LYP/6-31G* using Gaussian, [b] HOMO and LUMO energy levels were calculated according to equations: $-(4.8+E_{ox}^{onset})$ and LUMO = HOMO + E_g, [c] $E_{ox}^{1/2}$ is the half-wave potential of the oxidative waves, [d] E_{ox}^{onset} is the onset potential of the first oxidative wave, with potentials *versus* Fc/Fc⁺ couple. [e] E_g: estimated from UV-vis absorption spectra in solution. nd. No determination.